Energy & Buildings 354 (2026) 116925

Contents lists available at ScienceDirect

Energy & Buildings

journal homepage: www.elsevier.com/locate/enbuild

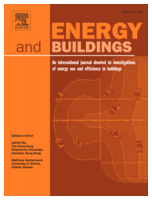

Cross-domain indoor performance prediction via in-context learning: A CFD-TabPFN-SHAP framework integrating air quality, energy, and thermal comfort

Xueren Li [a,b,c], Weijie Sun [d,*], Liwei Zhang [e], Bichen Shang [e], Ruipeng Xu [f], Jiyuan Tu [c,*], Yuanfu Pei [g], Xiang Fang [h]

[a] School of Safety Engineering, China University of Mining and Technology, Xuzhou, 221116, China
[b] Jiangsu Engineering Research Center of Dust Control and Occupational Protection, Xuzhou, 221008, China
[c] School of Engineering, RMIT University, PO Box 71, Bundoora, VIC, 3083, Australia
[d] Department of Computing Science, University of Alberta, Edmonton, AB, T6G 2R3, Canada
[e] School of Mechanical Engineering, Purdue University, West Lafayette, USA
[f] Department of Chemical Engineering, Faculty of Applied Sciences, Delft University of Technology and J.M. Burgerscentrum Research School for Fluid Mechanics, Van der Maasweg 9, 2629, HZ Delft, The Netherlands
[g] Gansu Beautiful Technology Industrial Group Co., Ltd, Gansu, China
[h] School of Mechanical and Automotive Engineering, Shanghai University of Engineering Science, 201620, China

ARTICLE INFO

Keywords:
Indoor air
Thermal comfort
Energy use
TabPFN
Machine learning prediction
In-context learning

ABSTRACT

Efficient indoor environmental management is vital for reducing energy use while safeguarding indoor air quality and occupants' comfort. However, due to difficulty of obtaining comprehensive datasets across multiple domains, many current studies still focus on a single performance metric, with dataset limitations preventing the development of robust and accurate multi-objective predictive models and operate as opaque data-driven systems with limited explanatory capability. This work developed CFD datasets derived from an experimentally validated model to systematically generate data covering parameters of indoor air quality, energy use, and thermal sensation with varied ventilation conditions. This dataset is further used for machine learning (ML) analysis. A cutting-edge Tabular Prior-data Fitted Network (TabPFN) is adopted for multi-target prediction and benchmarked against XGBoost, CatBoost, and Backpropagation Neural Networks (BPNN). SHapley Additive exPlanations (SHAP) method was used to elucidate its predictions, identifying how the most influential parameters govern the variations in indoor environmental behavior. The findings indicate that TabPFN outperforms the other three models in both predictive accuracy and computational efficiency, with MAE reduced by 62.08-95.4 % and RMSE by 49.15-85.50 %, while inference is accelerated by 67.5-85.9 %. SHAP analysis quantified nonlinear and directional contributions of features, linking model outputs to physical mechanisms such as draft risk, thermal sensation, and cooling load demand. The proposed TabPFN-SHAP framework is expected to offer valuable insights to guide the optimisation of building environmental control strategies.

1. Introduction

Increasing demands for urbanisation have been revealed in recent years, with estimates suggesting that nearly 600 million additional people will reside in urban areas by 2030 [1]. A substantial portion of this demand directly drives increasing energy consumption in the building sectors including heating, cooling, lighting and other services, which together account for nearly 40 % of global energy use [2,3]. As modern populations spend almost 90 % of their time in enclosed settings, whether in residential buildings, offices, or commercial spaces, the built environment continues to play a vital role in ensuring indoor air quality (IAQ) and thermal sensation for optimal productivity and well-being [4]. However, simultaneously achieving an optimal indoor environment from across these three aspects (i.e., IAQ, energy and thermal comfort) still poses significant challenges. While substantial energy use is expended to maintain indoor environmental quality, inefficient environmental control strategies often lead to excessive energy consumption, suboptimal thermal comfort, and compromised IAQ [5,6]. It has

* Corresponding authors.
E-mail addresses: xueren.li@hotmail.com (X. Li), weijie2@ualberta.ca (W. Sun), zhan5483@purdue.edu (L. Zhang), bshang@purdue.edu (B. Shang), R.Xu@tudelft.nl (R. Xu), jiyuan.tu@rmit.edu.au (J. Tu), pyf6546@163.com (Y. Pei), xiang.fang@sues.edu.cn (X. Fang).

https://doi.org/10.1016/j.enbuild.2025.116925
Received 25 October 2025; Received in revised form 14 December 2025; Accepted 27 December 2025
Available online 5 January 2026

Nomenclature -		***Greek symbols*** -	
S	Source term	μ	Turbulent viscosity $[\mathrm{kg}\cdot\mathrm{m}^{-1}\cdot\mathrm{s}^{-1}]$
T	Temperature [°C]	ν	Kinetic viscosity $[\mathrm{m}^2\cdot\mathrm{s}^{-1}]$
C_p	Specific heat at constant pressure	τ	Local Mean Age of Air [s]
U	local mean air velocity [m/s]	ρ	Density $[\mathrm{kg}\cdot\mathrm{m}^{-3}]$
Tu	local turbulence intensity [%]	λ	Parameter Scales the Penalty Associated with the Complexity
Re	Reynolds number	γ	Cost Related to Complexity of Adding New Leaves to Trees
M	Metabolic Rate $[\mathrm{W}\cdot\mathrm{m}^{-2}]$	***Subscripts***	
W	External Work$[\mathrm{W}\cdot\mathrm{m}^{-2}]$	f	Fluid
$\mathrm{h_c}$	Convective Heat Transfer Coefficient $[\mathrm{W}\cdot\mathrm{m}^{-2}]$	i	Direction
$\mathrm{I_{cl}}$	Thermal resistance of the clothing	eff	Effective
R^2	R-squared	u	Local
s	Tangent Sigmoid Function	ref	Reference
Q_{coil}	Cooling Coil Load	cl	Clothing
Q_{space}	Space cooling load	***Abbreviation***	
T_e	Exhaust Temperature	ML	Machine Learning
T_f	Fresh Air Temperature	GA	Genetic Algorithms
$\dot{m}_\mathrm{f}$	Fresh Air Flow Rate	PSO	Particle Swarm Optimisation
$\dot{m}_\mathrm{e}$	Exhaust Air Flow Rate	$TabPFN$	Tabular Prior-data Fitted Network
w_{ij}	Initial Wight	CNN	Convolutional Neural Networks
H_j	Hidden Layer Vector	DT	Decision Tree-Based Models
PPD	Predicted Percentage of Dissatisfaction	GBM	Gradient Boosting Machines
SCM	Structural Causal Models	RF	Random Forest
PMV	Predicted Mean Vote	$BPNN$	Back Propagation Neural Networks
MAE	Mean Absolute Error	$XGBoost$	eXtreme Gradient Boosting
$RMSE$	Root Mean Squared Error	$CatBoost$	Categorical Boosting
$SHAP$	SHapley Additive exPlanations	ANN	Artificial Neural Networks

been reported that overall occupant satisfaction is still limited, i.e., only around 80 % of occupants report comfort in roughly one-quarter of assessed buildings [7]. Therefore, there is an urgent need for more efficient and adaptive environmental control strategies that can dynamically regulate indoor conditions while minimising energy consumption.

Before indoor environments can be optimised using novel environmental control strategies or techniques, it is necessary to first evaluate and predict air quality, energy use and thermal comfort [8]. Simulation tools, such as TRNSYS [9], EnergyPlus [10], etc, are widely used for this purpose, with computational fluid dynamics (CFD) being particularly popular due to its ability to provide detailed, intuitive and quantitative analyses of airflow distribution, pollutant dispersion and thermal conditions from indoor scales [11,12] to urban scales [13,14]. For instance, Xi, et al. [15] used CFD to analyse the impinging jet ventilation performance in an office by coupling the thermal and moisture transfer effects. Mahecha Zambrano and Baldini [16] developed a CFD-coupled thermoregulation framework to assess thermal comfort in spatially non-uniform indoor environments. Feng, et al. [17] visualised aerosol spread in face-to-face meeting scenarios and introduced an air-curtain-based strategy to mitigate infection risks among occupants. Regarding energy consumption, Qin, et al. [18] parametrically evaluated the effect of return vent height in a room with stratified air ventilation, accounting for varying cooling coil loads. These studies demonstrate the critical role of CFD in indoor environment design. Nevertheless, achieving high-fidelity CFD solutions typically requires refined mesh elements, reduced time-step sizes to resolve transient behavior, and complex multiphysics/multiphase coupling [19,20]. These factors inevitably result in prohibitively high computational costs and processing times, making real-time control infeasible. Given this pressing need, alternative approaches that offer faster, more efficient, and adaptable predictive capabilities are essential and thus worth developing.

Machine learning (ML) techniques have been increasingly utilised in building environmental studies for prediction and optimisation purposes, frequently in conjunction with algorithms, e.g., Genetic Algorithms (GA) [21]. Various ML models, including Convolutional Neural Networks (CNNs) [22], Decision Tree-Based Models (DTs) [23–26], Artificial Neural Networks (ANNs) [27], etc, have been widely applied to estimate indoor air quality (IAQ) indicators (e.g., CO_2 concentration [28], particulate matter levels [29], ventilation effectiveness [30], air pollutant concentrations [31]), thermal comfort indices (e.g., Mean Vote (PMV) [32], comfort duration [33], temperature [34], humidity [35]), and energy indicators (e.g., HVAC energy consumption [36,37], total building energy demand [38], operational efficiency [39]). These models can capture complex nonlinear relationships among environmental parameters and deliver rapid predictions, making them valuable tools for guiding ventilation strategies, HVAC control, and building design [40]. Despite those efforts, most aforementioned ML-based studies have primarily addressed only a single dimension of indoor environmental performance and thus may not keep pace with the rising need for designing advanced building envelopes. There is increasing evidence indicating that, for intelligent and advanced building operations, indoor air quality, energy use, and thermal comfort should be optimised simultaneously [41]. However, in real-world settings, such multi-dimensional data are rarely collected simultaneously, which often leads to fragmented and limited datasets [42]. Therefore, to holistically achieve optimal indoor environment control, a predictive framework that can effectively handle multi-target prediction and remain reliable under limited data availability is required. In addition, it is also worth noting that simultaneously optimizing these three aspects requires identifying the most influential factors from a large set of monitored parameters and performance indicators. Even though ML algorithms can capture such nonlinear couplings through their powerful approximation capabilities, their black-box nature may hinder our ability to interpret the predictive information. Therefore, incorporating the interpretability of predictive models becomes essential.

To address the aforementioned research gaps, this study proposed a novel predictive and explainable framework based on the emerging in-context learning foundation model, i.e., Tabular Prior-data Fitted Network (TabPFN), coupled with SHapley Additive exPlanations (SHAP). TabPFN, a transformer-based model pre-trained to perform Bayesian

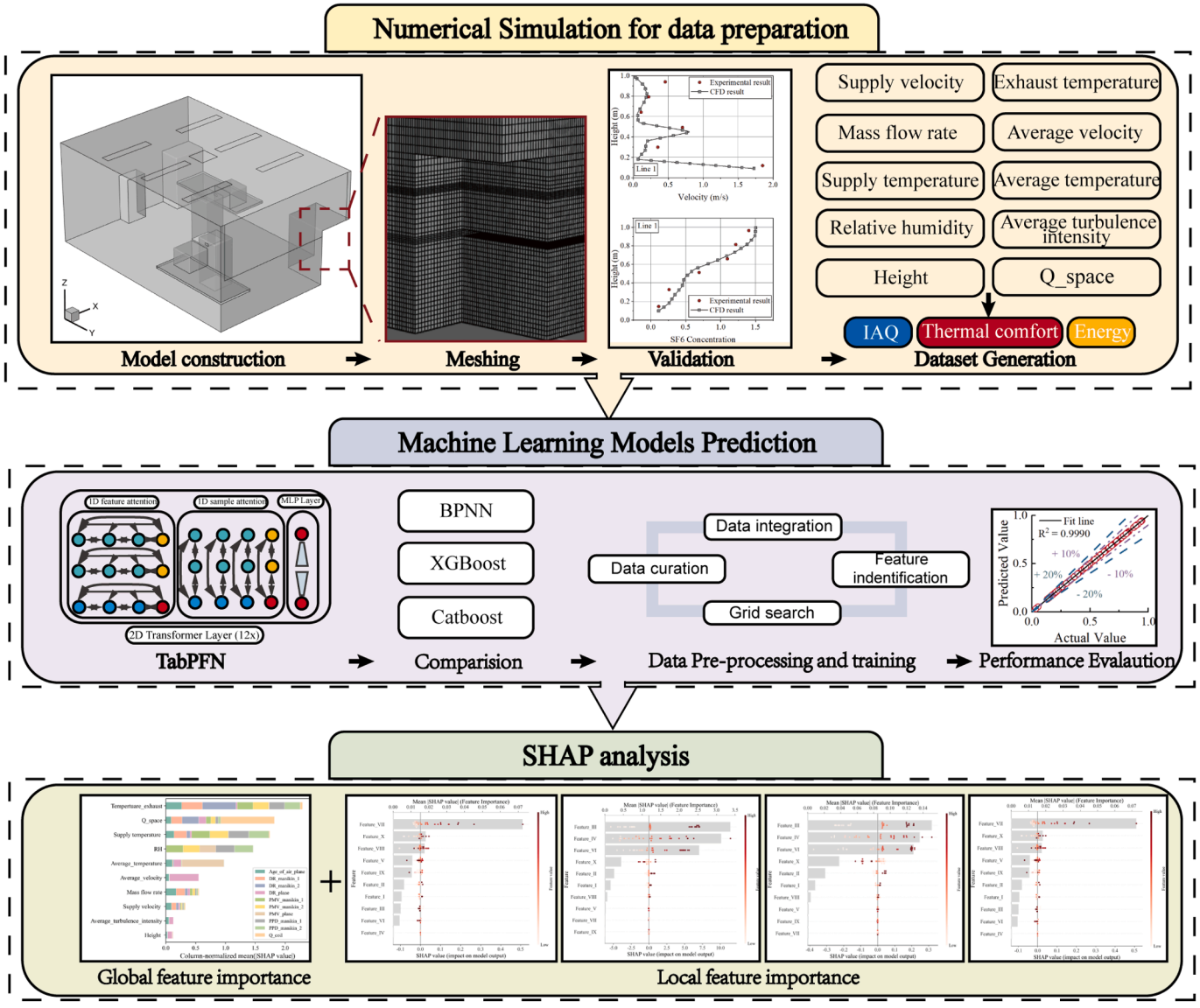

Fig. 1. Overall workflow in this study.

inference, has demonstrated strong predictive capabilities for small-sample tabular datasets [43]. To our knowledge, the application of TabPFN within the building domain has not yet been investigated, suggesting its potential for advancing predictive accuracy and optimisation in this field. To evaluate the robustness of the proposed framework, a validated CFD dataset was first developed to systematically generate multidimensional data, including IAQ, energy use and thermal comfort under various environmental and operational conditions. Such a dataset was used to train TabPFN, and its predictive performance was compared against those widely adopted ML models, including the BPNN, XGBoost and CatBoost. Finally, the SHAP method was employed to elucidate model predictions, enabling the identification of influential variables and uncovering deeper physical insights into the mechanisms governing indoor environmental dynamics. This study is expected to shed light on developing a predictive and explainable framework for multi-target, cross-domain indoor performance.

2. Methodology

The overall workflow in this study involved the generation of a validated CFD-based dataset, training and benchmarking the TabPFN model against established ML methods, and applying SHAP analysis to interpret multi-target indoor environmental predictions, as demonstrated in Fig. 1.

2.1. Model description and simulation details

In this work, the model validation was based on experimental data reported in the existing literature, which were obtained from a ventilation operation experiment, i.e., an office room layout resembling a displacement ventilation system [44]. Fig. 2(a) demonstrates the overall configuration of the environmental test facility used in the literature, which aimed to provide a macroscopic view of the experimental chamber and its HVAC systems. In the experiments, the ventilation performance in a specific two-person office arrangement within the test chamber was performed, as demonstrated in Fig. 2(b). In the experimental setup, a perforated exhaust outlet was centrally mounted on the ceiling, whereas a perforated displacement diffuser (0.5 m × 1.1 m) was placed near the floor along the right-hand wall. The rectangular thermal manikin (0.4 m × 0.35 m × 1.1 m) was used to simulate an occupant, with a heating source of 75 W. Two personal computers (108 W and 173 W) served as additional heat sources. Each overhead fluorescent

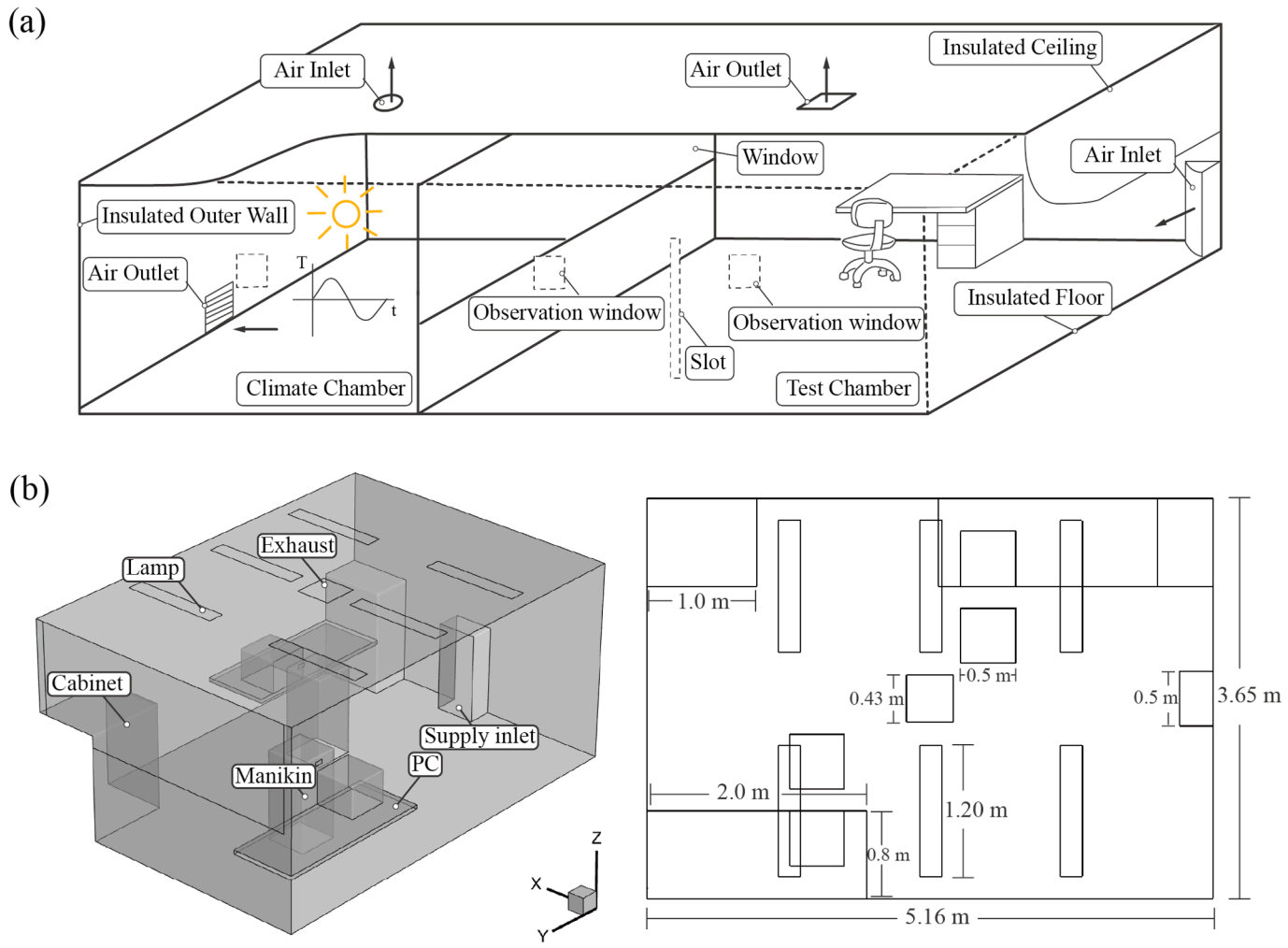

Fig. 2. (a) Experiment model and (b) Numerical model of a office room and its detailed dimensions [44].

lamp provided an electrical power density of 34 W/m^2 for illumination. The ventilation rate was set at 4 ACH, with an inlet velocity of 0.09 m/s and temperature of 17.0°C. To validate the results attained from the experimental measurements in the existing literature, a physical model of an office room with the same layout and configuration was numerically built, as demonstrated in Fig. 2(b).

To simulate the turbulent flow induced by displacement ventilation, this work used RNG k-epsilon model. The thermal buoyancy flow induced via manikin body heat was modelled using the Boussinesq approximation. The physical model was discretised with structured hexahedral mesh using the ANSYS ICEM Mesh 2022 R1, as shown in Fig. 3(a).

All of the boundary conditions was set according to those found in the experimental study. To verify mesh independence, four computational grids with total cell counts of about 0.6, 1.1, 1.9, and 3.2 million were examined in this study. The mesh quality was first checked, and the grid convergence index was further examined. Furthermore, velocity information along several randomly selected locations was used as the indicator for the mesh independence test. Fig. 3(b) reveals that the velocity distribution changed insignificantly when the mesh density was increased from 1.9 to 3.2 million elements. Therefore, the mesh configuration of 1.9 million was finally selected.

In this study, the training dataset was generated from a series of CFD simulations of an indoor space equipped with displacement ventilation. To evaluate the robustness of the ML-based models, key variables were parametrically varied, resulting in a total of 36 case scenarios. The outlines of cases performed in this work can be found in Table 1.

Table 1
Training variables combination used in this study.

Supply velocity (m/s)	Supply temperature (°C)	Relative humidity (%)
0.015, 0.045, 0.09	16 20, 24, 28	10, 30, 50, 70, 90

2.2. Performance evaluation metrics for ventilation

In the study, the ventilation performance consisted of several commonly adopted criteria, listed as the age of air (MAA), the Predicted Mean Vote (PMV), draught rating index (DR), the Predicted Percentage of Dissatisfied (PPD) and energy consumption.

2.2.1. Age of air

The local mean age of air (MAA) serves as an important indicator of indoor air quality (IAQ), describing the average residence time of airflow from the inlet to a given point within the occupied space [45]. A higher MAA indicates areas where air is not effectively ventilated, potentially leading to poorer air quality. The governing equation for MAA can be written as follows:

$$\rho\frac{\partial \tau u_j}{\partial x_j} = \frac{\partial}{\partial x_j}\left[\left(2.88\rho\times 10^{-5} + \frac{\mu_{eff}}{Sc_t}\right)\frac{\partial \tau}{\partial x_j}\right] + S_\tau \quad (1)$$

Here, τ refers to the local mean age of air (MAA), μ_{eff} indicates the effective turbulent viscosity, and S_τ stands for the source term. This formulation was incorporated into the solver via a user-defined function.

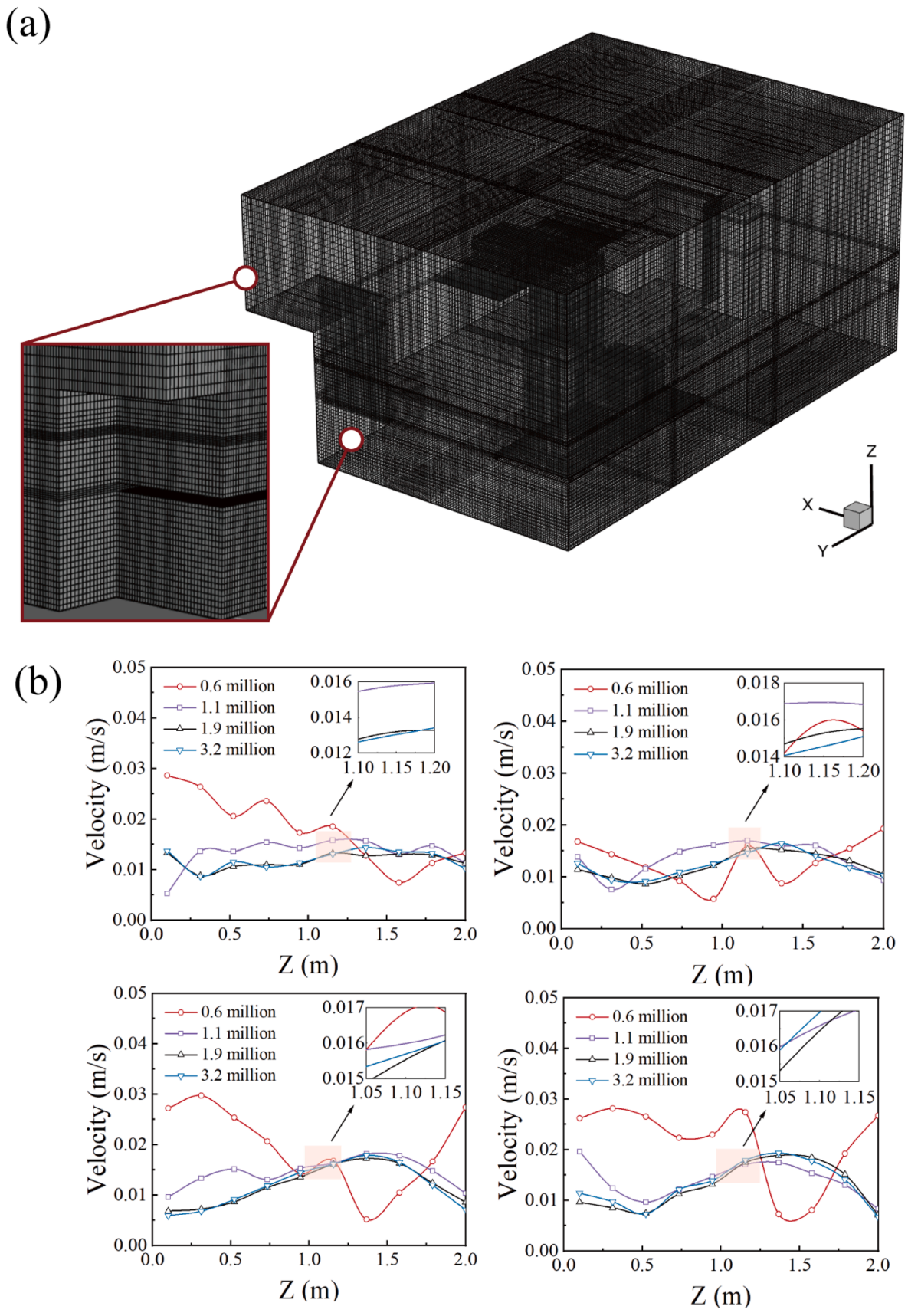

Fig. 3. (a) Mesh information and (b) Mesh independence test.

2.2.2. Draught rating index (DR)

In this study, air quality and comfort are used in a broad sense to cover airflow-related indicators, including both the age of air (ventilation effectiveness) and draft rate (local air movement discomfort) [46,47]. Draft rate is a widely used index to quantify the risk of local discomfort caused by unwanted air movement in indoor spaces. The DR is written as:

$$DR = (34 - T_a)(U - 0.05)^{0.62}(0.37 \cdot Tu + 3.14) \tag{2}$$

The parameters include the air temperature (T_a, °C), the local mean air velocity (U, m/s), and the local turbulence intensity (Tu, %). The turbulence intensity is quantified according to the following equation:

$$T_u = 0.16Re^{-0.125} \tag{3}$$

where Re is defined as Reynolds number.

2.2.3. PMV and PPD

Thermal perception terms such as "cold," "cool," "neutral," and "warm" describe an occupant's subjective experience of temperature [48]. In contrast, thermal comfort is an objective measure, characterised as "pleasant" or "unpleasant." The Fanger model, widely used in built environments, relies on PMV and PPD [49,50]. These indices use steady-state temperature, environmental variables, and clothing insulation to estimate the average thermal response of occupants. For acceptable thermal conditions, PMV should range between -1 and +1, with an optimal comfort range of -0.5 to +0.5. The key equation of PMV can be written as:

$$PMV = [0.303\exp(-0.036M) + 0.028] \times \left\{ \begin{array}{c} (M - W) - 3.05 \times 10^{-5} \\ \times[5733 - 6.99(M - W) - P_a] \\ -0.42 \times [(M - W) - 58.15] \\ -1.7 \times 10^{-5} \times M \times (5867 - P_a) \\ -0.0014M \times (34 - T_a) \\ -3.96 \times 10^{-8} \times f_{cl} \\ \times\left[(T_{cl} + 273)^4 - (T_r + 273)^4\right] \\ -f_{cl} \times h_c \times (T_{cl} - T_a) \end{array} \right\} \tag{4}$$

In this formulation, M stands for the metabolic rate (W/m^2), W for the external work (W/m^2), T_a for the air temperature (°C), h_c for the convective heat transfer coefficient (W/(m^2 ·° C)), and I_{cl} for the thermal resistance of clothing (m^2 ·° C/W).

The PPD based on PMV value can be expressed as

$$PPD = 100 - 95\exp\left(-0.03353PMV^4 - 0.2179PMV^2\right) \tag{5}$$

2.2.4. Energy consumption

This work adopted the cooling coil load, Q_{coil} , to quantify the energy use of the ventilation system. The index is extensively utilised for assessing exhaust-return configurations [11], with its formulation given as follows:

$$Q_{coil} = Q_{space} - c_p\dot{m}_f(T_e - T_f) \tag{6}$$

Here, Q_{space} denotes the space cooling load, which includes both internal heat sources and external heat transfer through the walls. T_f ans T_e represent the fresh and exhaust air temperatures, respectively. For airtight spaces, fresh air mass flow rate ($\dot{m}f$) is equal to the exhaust air ($\dot{m}e$). The corresponding schematic layout is illustrated in Fig. 4.

2.3. Machine learning models

This study used TabPFN, a cutting-edge foundation model designed for small tabular datasets, as the benchmark framework for multi-target prediction of indoor environmental performance in order to address the difficulty of producing accurate and interpretable predictions with a limited small training dataset. Three popular machine learning algorithms,

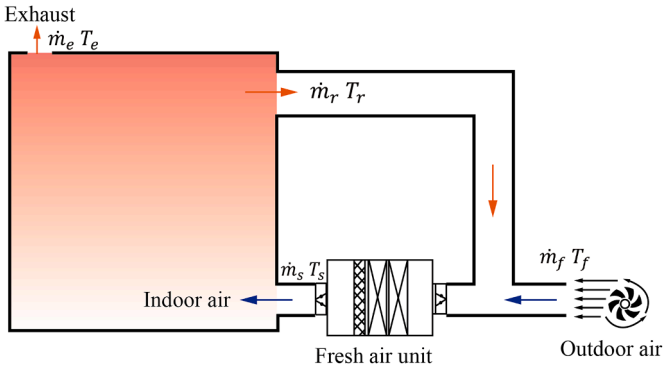

Fig. 4. Stratified air distribution system.

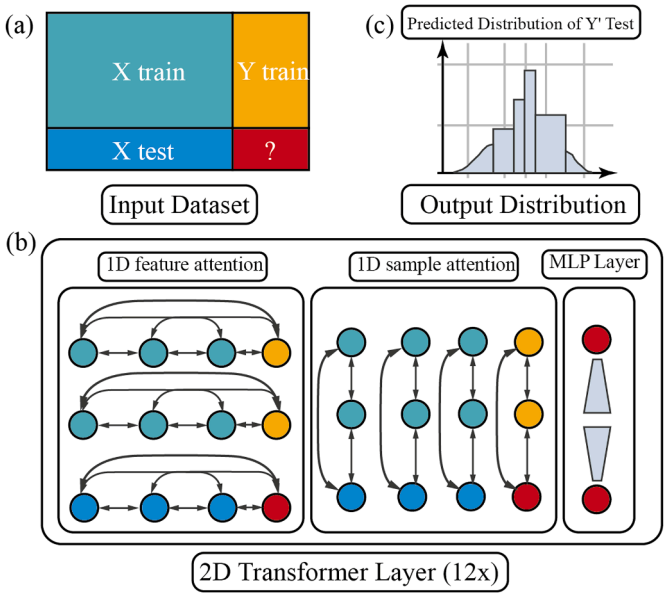

Fig. 5. Schematic diagram of the TabPFN.

i.e., BPNN, XGBoost, and CatBoost, are used for comparison in order to methodically assess its performance. The SHAP (SHapley Additive exPlanations) method was subsequently used to improve outcome interpretability and determine the key physical parameters that govern changes in energy use, indoor air quality, and thermal comfort.

2.3.1. TabPFN model

We use TabPFN, a transformer-based meta-learner that approximates the Bayesian posterior predictive for small- to medium-sized tabular tasks [43,51]. During pretraining, the model is exposed to a very large corpus (about 1.3×10^8) of synthetically generated datasets sampled from a prior over data-generating mechanisms instantiated via structural causal models (SCMs).

At inference, we serialise the support set (X_{train}, Y_{train}) and the queries X_{test} into a single sequence and feed it to the transformer under a block-causal attention mask, such that each query can attend to all support items (features and labels) but not to other queries nor to any query labels. In a single forward pass-without any gradient updates on the target dataset-the model outputs for each query x^* a predictive density

$$\hat{p}_\theta(y^* \mid X_{train}, Y_{train}, x^*) \tag{7}$$

For our regression task, we follow the TabPFN formulation: apply a monotone transform T to the targets (z-score with an optional Yeo–Johnson/power transform), and parameterise on the T-space a *piecewise-constant* predictive density by assigning probabilities to B contiguous

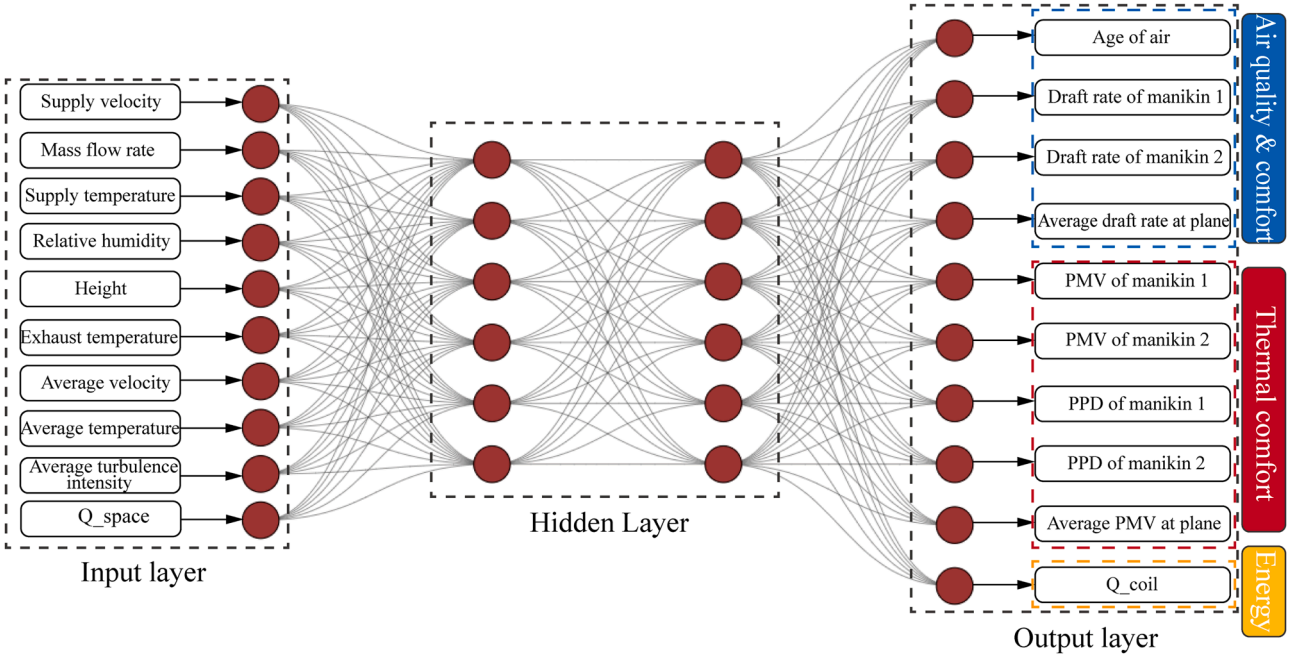

Fig. 6. Multi-output BPNN model architecture used in this study.

quantile bins, augmented with *half-normal* tails to ensure full support. Writing the bin borders as $\{b_k\}_{k=0}^{B}$ and the predicted bin probabilities as $\{\pi_k\}_{k=1}^{B}$ (via a softmax), the predictive density over $T(y)$ is

$$p\big(T(y) \mid X_{\text{test}}, X_{\text{train}}, Y_{\text{train}}\big) = \sum_{k=1}^{B} \pi_k \frac{\mathbb{I}\{T(y) \in [b_{k-1}, b_k)\}}{b_k - b_{k-1}} + p_{\text{tail}}\,(T(y)), \tag{8}$$

where p_{tail} denotes the half-normal tails attached to the outermost bins. The final predictive density on the original scale is obtained via the change of variables $p(y) = p(T(y))\,|T'(y)|$. In practice, we report point estimates (e.g., mean or median under $p(y)$) and prediction intervals from its cumulative mass.

Fig. 5 demonstrates the schematic diagram of TabPFN. As shown in Fig. 5(a), the inference process concatenates the context set $C = (X_{\text{train}}, Y_{\text{train}})$ with the query inputs X_{test} to predict the corresponding outputs Y_{test}. The backbone network, depicted in Fig. 5(b), consists of a stack of two-dimensional transformer layers, where each layer sequentially performs column-wise (feature-level) self-attention and row-wise (sample-level) self-attention, followed by a position-wise multilayer perceptron. All sublayers incorporate residual connections and half-precision layer normalisation. In this work, we used 12 such layers, and this alternating row/column attention structure enables the model to jointly capture inter-feature and inter-sample dependencies. Finally, as highlighted in Fig. 5(c), the prediction head outputs a piecewise-uniform density distribution over quantile bins in a normalised target space with half-normal tails; an inverse transformation is subsequently applied to recover the predictive density in the original scale.

2.3.2. Backpropagation neural network (BPNN)

BPNN model has been widely used for predicting complex and non-linear variables in the field of built environments. As building design continues to incorporate an increasing number of variables for consideration, a robust surrogate model must effectively handle multiple input and output variables. In this study, we evaluated the predictive capability of BPNN in managing a large set of input and output variables, assessing its suitability as a versatile alternative model for future design applications. Fig. 6 shows that the input layer consists of supply velocity, mass flow rate, supply temperature, relative humidity, exhaust temperature, average velocity, temperature, and turbulence intensity at the given height, and Q_{space}. The outputs consist of the age of air, draft rate and PMV/PPD for each manikin, average draft rate and PMV at the given plane, and Q_{coil}.

During training, initial weights (w_{ij}) and biases (b_j) between the input and hidden layers are randomly assigned to establish the connections between these layers. The hidden layer vector H_j is computed as:

$$H_j = \sum_{i=1}^{n} w_{ij} x_i + b_j \tag{9}$$

where $W = (w_{1j}, w_{2j}, \ldots, w_{nj})$ represents the weights between the hidden layers and input layers. The hidden layer employs a tangent-sigmoid activation function (S), mathematically defined as:

$$s_j = \frac{1 - e^{H_j}}{1 + e^{H_j}} \tag{10}$$

2.3.3. eXtreme gradient boost (XGBoost) and categorical boosting (CatBoost)

XGBoost, developed by Chen and Guestrin [52], introduced regularisation term into the objective function to smooth the ultimate learning weights and reduce the risk of overfitting [53,54]. In this study, the training and predictive variables of XGBoost were as same as those for the BPNN model. The objective function of XGBoost is formulated as follows:

$$\text{Obj}(\phi) = \sum_{i=1}^{n} l\big(y_i, \hat{y}_i\big) + \frac{1}{2}\lambda \sum_{q=1}^{Q} w_q^2 + \gamma Q \tag{11}$$

Here, l denotes a differentiable convex loss function that quantifies the difference between the target value y_i and the predicted output $\hat{y}_i$. The variable n represents the total number of samples in the dataset. The coefficient λ controls the strength of the regularisation term by scaling the penalty imposed on model complexity and the weight parameters w_q. The term γ corresponds to the cost associated with adding additional leaves to the trees. A schematic illustration of the XGBoost framework is provided in Fig. Fig. 7(a).

A recent algorithm for gradient boosting called CatBoost, which is designed to efficiently handle categorical variables while reducing

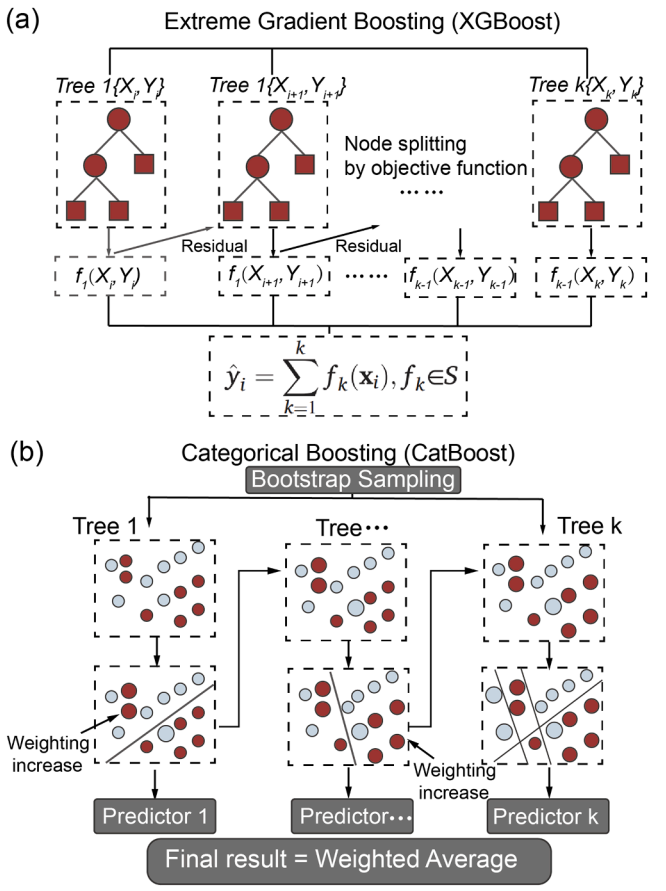

Fig. 7. Schematic diagram of the decision-tree based model (a) XGBoost and (b) CatBoost.

overfitting and improving generalisation [55]. Categorical features consist of distinct values that cannot be directly utilised in binary decision trees, often requiring transformation into numerical representations through methods like one-hot encoding. Unlike traditional boosting methods, CatBoost assigns increased weighting to misclassified instances as trees are sequentially trained. Each tree refines predictions based on prior errors, and the final output is computed as a weighted average of all predictors, enhancing accuracy while reducing overfitting [56]. A schematic illustration of the CatBoost framework is provided in Fig. 7(b).

2.3.4. Interpretability analysis based on SHAP

Currently, ML-based surrogate modeling techniques are typically regarded as black-box approaches that offer little transparency regarding their internal functioning. To address this limitation, this work applied SHapley Additive exPlanations (SHAP) analysis to quantitatively reveal the contributions and directionality of each input feature to model predictions.

SHAP analysis originates from Shapley value theory [57], ensuring a consistent and equitable allocation of feature contributions. The method determines each feature's effect on a specific prediction by contrasting model outputs that include or exclude the feature in question. To obtain the global feature importance, the weighted average of each feature's contribution across all instances was computed.

2.3.5. Evaluation metrics and hyperparameter determination

To obtain optimal predictive outcomes, a grid search strategy was applied to determine the optimal hyperparameters of each model. Five-fold cross-validation was applied to evaluate model performance, and the configuration yielding the minimum validation loss was identified as optimal.

Model evaluation was performed by adopting widely used error metrics. Model evaluation was conducted using several widely adopted error metrics. To assess the goodness of fit, we employed the coefficient of determination (R^2). To evaluate prediction accuracy, we used the Mean Absolute Error (MAE) and the Root Mean Squared Error (RMSE), both of which provide consistent and interpretable absolute error measurements. The definitions of these metrics are summarised below:

$$MAE = \frac{1}{n}\sum_{i=1}^{n}|y_i - \hat{y}_i| \tag{12}$$

$$RMSE = \sqrt{\frac{1}{n}\sum_{i=1}^{n}(y_i - \hat{y}_i)^2} \tag{13}$$

$$R^2 = 1 - \frac{\sum(y_i - \hat{y})^2}{\sum(y_i - \bar{y})^2} \tag{14}$$

Here, y_i denotes the observed value, $\hat{y}_i$ represents the predicted value, and $\bar{y}$ indicates the mean of y. The symbol n refers to the total number of samples.

For the experimental setup, fixed data splits for training, validation, and testing were used. The full dataset was randomly divided into a 75 % development set and a 25 % held-out test set using a fixed random seed to ensure reproducibility. Hyperparameters for BPNN, CatBoost, and XGBoost were tuned on the development set via a comprehensive grid search. For each configuration, we conducted 5-fold cross-validation within the development set and selected the configuration with the best average cross-validation performance. The hyperparameter search spaces and the selected best hyperparameters are reported in the Appendix, as outlined in Table 3-5

For BPNN, the best configuration is a three-layer MLP with hidden sizes [256, 256, 128], GELU activations, no dropout, and no batch normalisation, trained with AdamW, learning rate 10^{-3}, weight decay 10^{-5}, batch size 64, and MSE loss. Training was run for at most 800 epochs with early stopping on the validation loss (patience 80, minimum improvement 10^{-5}), and the learning rate was reduced by a factor of 0.5 when the validation loss plateaus for 30 epochs. Both input features and multi-output targets were standardised using statistics computed on the training data, and predictions were inverse-transformed to the original target scale for evaluation. For CatBoost, the best configuration usesd depth 6, learning rate 0.03, L_2 leaf regularisation 10, `rsm` 0.8, and Bernoulli bootstrap with subsample 0.8, trained as a single multi-output `CatBoostRegressor` with the `MultiRMSE` loss/metric. For XGBoost, the best configuration used max_depth 4, learning rate 0.03, min_child_weight 1, subsample 0.8, colsample_bytree 1.0, reg_alpha 0.0, reg_lambda 1.0, and gamma 0.0, with the `multi_output_tree` strategy for joint multi-target prediction.

After selecting the best hyperparameters via 5-fold cross-validation on the development set, we retrained BPNN, CatBoost, and XGBoost using the training subset of the development set and used the remaining 10 % as a validation set for early stopping. We then reported final performance on the held-out test set. For TabPFN 2.0, we follow training-free inference: the entire training portion of the development set was provided as in-context reference, and each test instance was queried without fine-tuning.

3. Results and discussions

3.1. Validation

To ensure the robustness of the simulated dataset, the validation was first performed, as demonstrated in Fig. 8.

Fig. 8(a) shows the extracted planes and lines for the purpose of comparison. For this validation case (supply velocity −0.09 m/s, supply temperature −17°C), the predicted velocity vectors along the mid-plane of

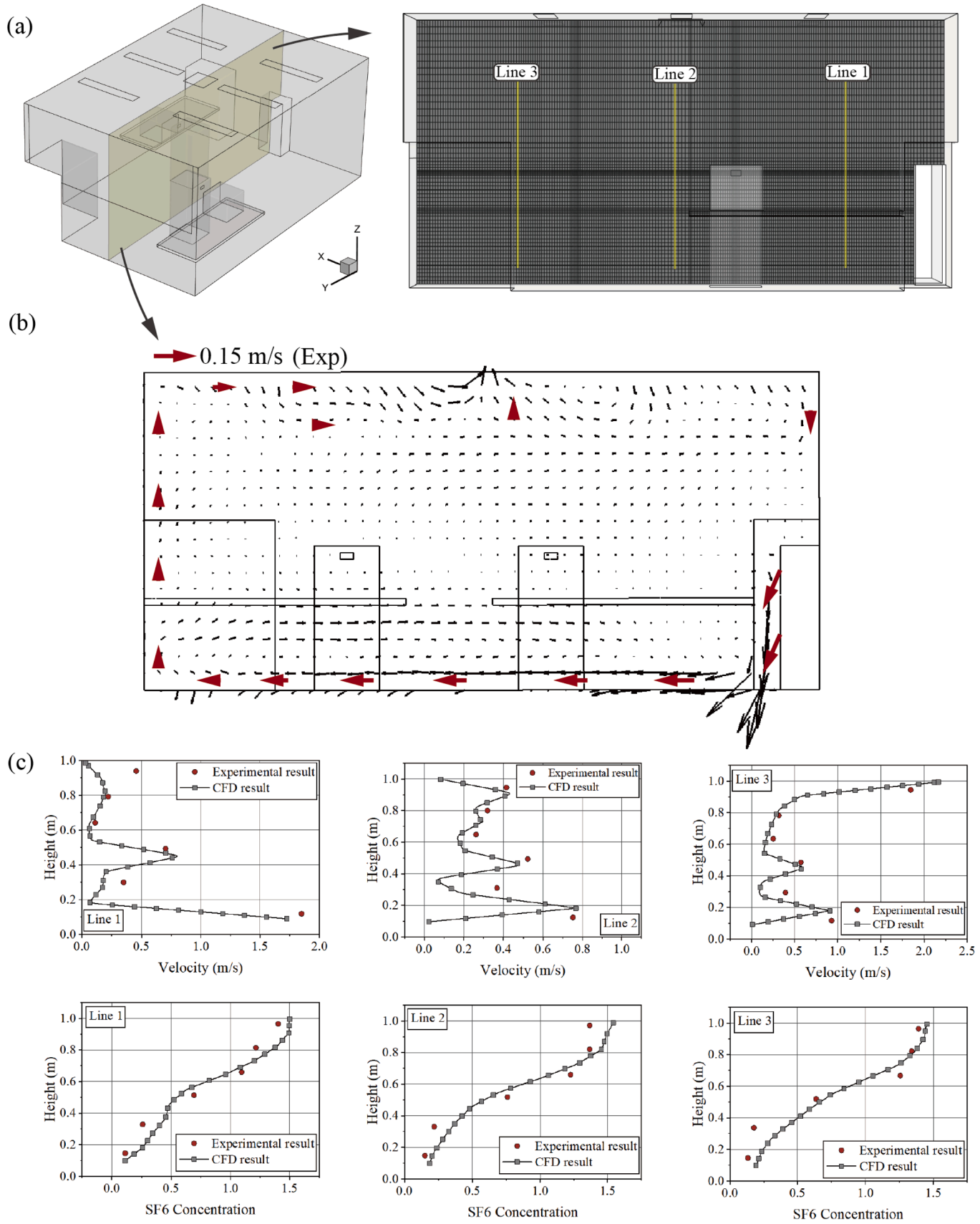

Fig. 8. Comparisons of CFD-predicted results with experimental measurements (a) Comparison line location, (b) airflow pattern comparison, and (c) velocity and contaminant concentration comparison.

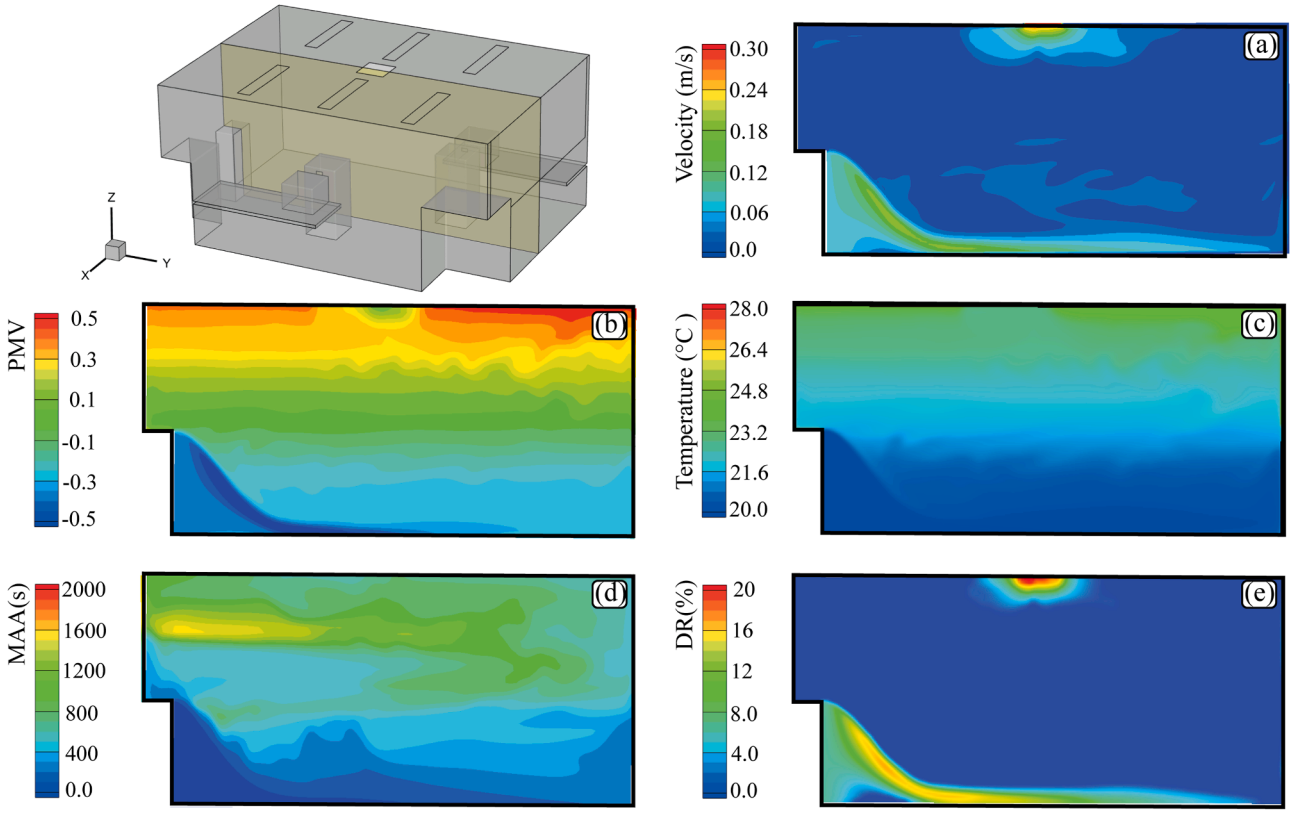

Fig. 9. Airflow field visualisation across the middle plane: (a) Velocity field, (b) PMV, (c) Temperature field, (d) MAA, and (e) DR.

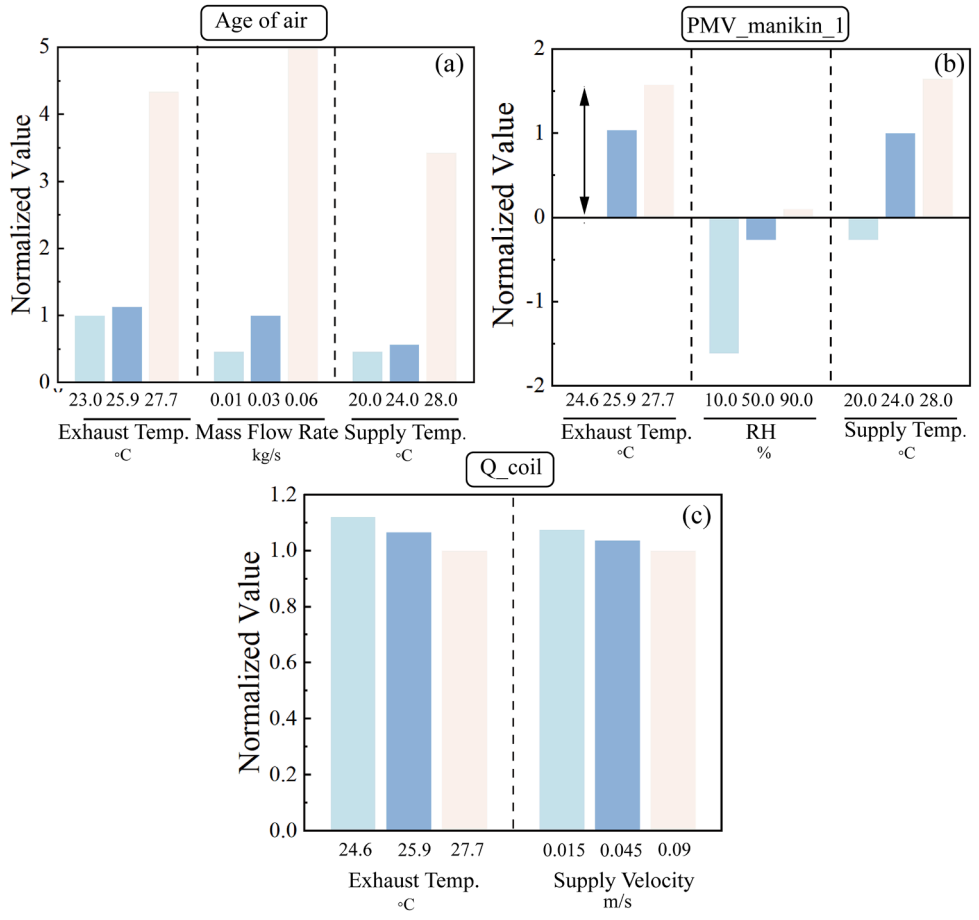

Fig. 10. Normalised responses of Age of air, PMV, and Q_coil under variations in key input variables.

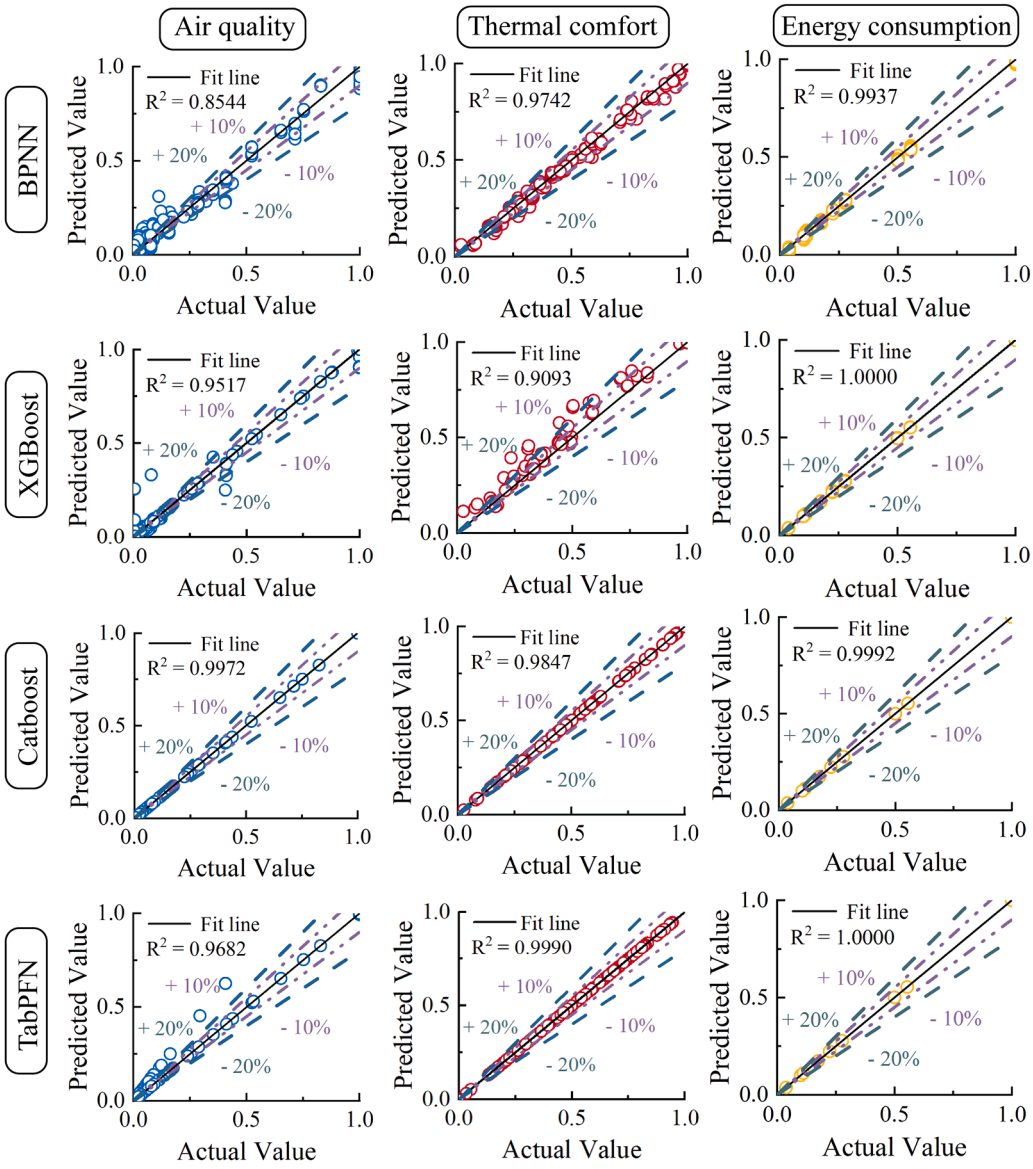

Fig. 11. Correlations between ML predictive and CFD outcomes.

the domain exhibited an airflow pattern consistent with the experimental observations, as illustrated in Fig. 8(b). Quantitatively, both the velocity and contaminant concentration profiles demonstrated satisfactory agreement between the simulation and experimental measurements, as shown in Fig. 8(c). The results proved the dataset attained from the numerical simulations can be trustworthy for the following machine learning analysis.

3.2. Airflow field visualisation

The airflow and indoor environment are shaped by displacement ventilation across the middle plane under the benchmark case (V_{inlet} = 0.09 m/s, T_{inlet} = 20ement ventilation across the middle plane under the benchmark case (V_{inlet} = 0.09 m/s, T_{inlet} = 20°C), as demonstrated in Fig. 9. The velocity field exhibits a typical displacement pattern, as seen in Fig. 9(a), with a stronger jet emerging close to the diffuser and low air speeds predominating in the occupied zone. By gently delivering fresh air at floor level, this design enables buoyancy forces from heat sources to propel upward motion. This stratification can be reflected in the PMV distribution shown in Fig. 9(b). While the upper zone gradually shifts toward warmer sensations, the lower occupied region stays near thermal neutrality (-0.5 to +0.5). This vertical gradient is supported by the temperature field in Fig. 9(c), which shows warmer air accumulating at the ceiling and cooler air near the floor. Fig. 9(d) showed the mean age of air measures the effectiveness of ventilation. Low air ages in the occupied zone indicate an efficient supply of fresh air, while higher values near the upper layers reveal limited mixing. Only a small area close to the diffuser experiences elevated draft risk values (Fig. 9(e)), with the majority of the occupied area remaining well below the 20 % threshold, indicating little discomfort from undesired air movement.

Fig. 10 further quantitatively revealed the representative indoor environmental indicators responding to controlled variations of major input variables, aiming to further verify the following SHAP analysis. Three indicators, i.e., the age of air, the PMV value of manikin 1, and Q_coil were adopted for the purpose of demonstration. For each variable examined, all remaining parameters were held constant to ensure that the observed trends reflect the isolated influence of the target variable. For the age of air, it can be found that sensitive variations were induced by temperature and mass flow rate. As this is a displacement ventilation system, the buoyancy-driven flow is predominantly influenced by

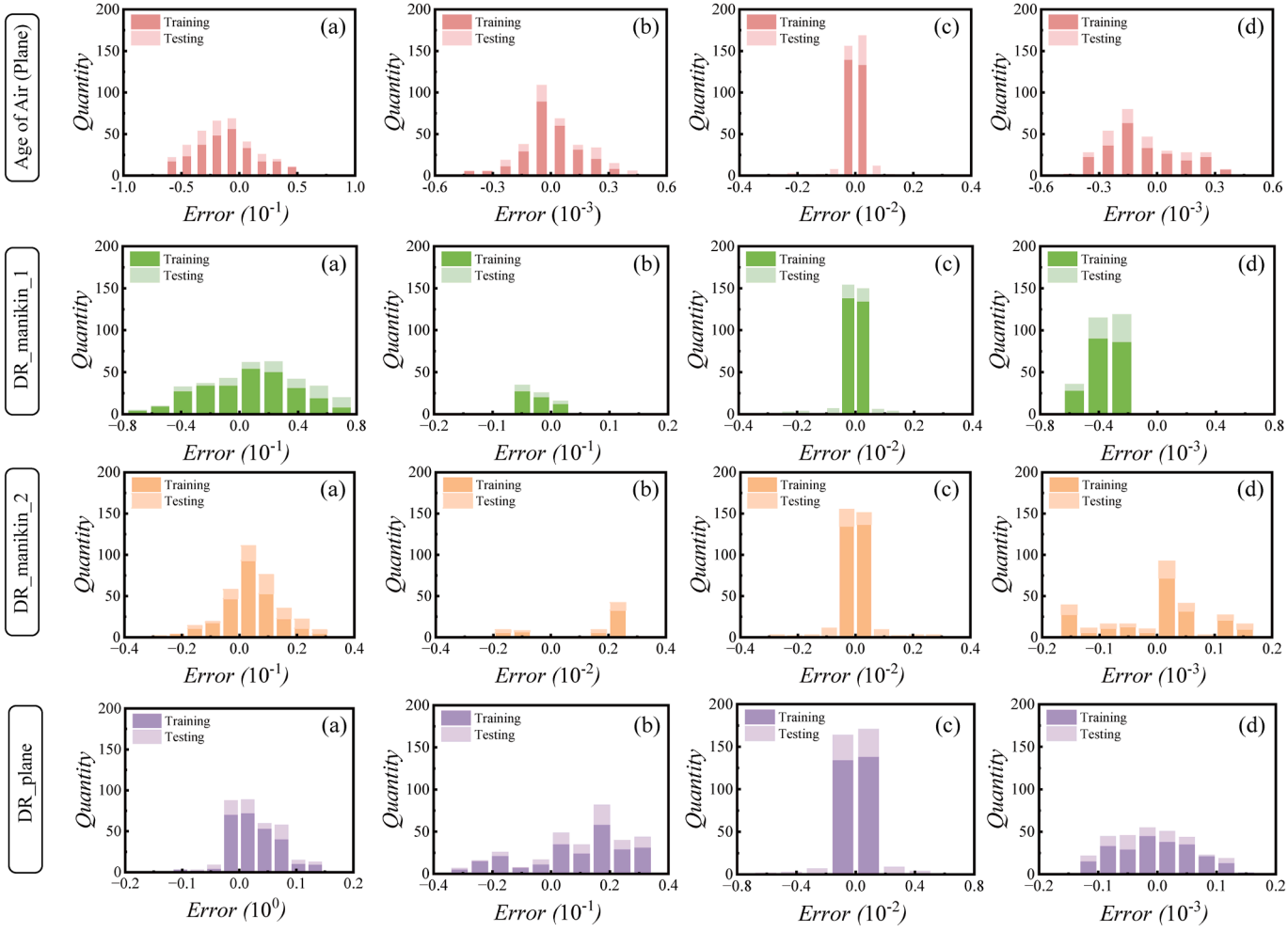

Fig. 12. Histogram-based comparison of prediction errors in air quality and thermal comfort estimation using four ML models-(a) BPNN, (b) CatBoost, (c) XGBoost, and (d) TabPFN.

the exhaust and supply temperatures. An increase of several degrees can lead to a rise in the age of air of up to approximately 4.2-fold. A reduction of the mass flow rate by up to 75 % results in almost a five-fold increase in the age of air, quantitatively demonstrating the strong nonlinear dependence of ventilation effectiveness on the volume of supplied fresh air. Fig. 10(b) further highlights the PMV variations under changes in RH and supply temperature. Increasing the supply temperature shifts PMV from near-neutral levels to approximately 0.98, while raising RH from 10 % to 90 % results in a comparable increase of roughly 1. These quantitative trends confirm that PMV is strongly governed by both sensible and latent heat exchange. For energy use, Fig. 10(c) revealed that the increase of exhaust temperature results in a reduction of Q_coil of up to nearly 11 %. This is because a higher exhaust temperature reduces the effective temperature difference available for sensible heat removal, thereby diminishing the net cooling demand that must be supplied by the coil [18]. Supply velocity, in this scenario, showed a relatively small influence on Q_coil, as changes in inlet momentum have only a minor effect on the overall room air temperature field and thus only weakly alter the cooling load [18].

3.3. Meachine learning results

In this study, four multi-target machine learning (ML) models, BPNN, XGBoost, CatBoost, and TabPFN, were employed to predict the overall indoor environmental conditions. Detailed input and output features referred to Fig. 6.

Since multiple variables were involved, all variables within each category were first normalised and then averaged to obtain the representative R^2 values shown in Fig. 11, which illustrates the prediction correlations of different models for each output category on the training dataset. It can be observed that for the training dataset, the R^2 values of all four models exceed 0.85, indicating that the machine learning models can effectively capture multiple indoor environmental objectives by explaining more than 85 % of the variance in the target indicators. The data points are also closely aligned with the identity line, confirming a strong agreement between the predicted and actual values. However, BPNN performed the worst overall, particularly for air quality indices, where its R^2 values dropped below 0.90. By contrast, TabPFN exhibited remarkable predictive accuracy across all categories, with R^2 values consistently ranging from 0.96 to nearly 1.0. Most notably, for energy consumption and thermal comfort indicators, TabPFN reached R^2 values close to 0.999, far surpassing the performance of BPNN and even slightly outperforming the strong baselines of XGBoost and CatBoost.

Figs. 12 and 13 illustrate the distributions of prediction errors obtained from four machine learning algorithms under both training and testing conditions for air quality, thermal comfort, and energy consumption metrics. BPNN and CatBoost produce the widest error distributions, which reflect larger prediction fluctuations and lower overall accuracy. XGBoost reduces the error range considerably, particularly for Age of Air Plane, Q_coil, PPD_manikin_1, PPD_manikin_2, DR_manikin_1, DR_manikin_2, and DR_plane, showing an order-of-magnitude improvement compared to BPNN. In contrast, TabPFN delivers the most compact

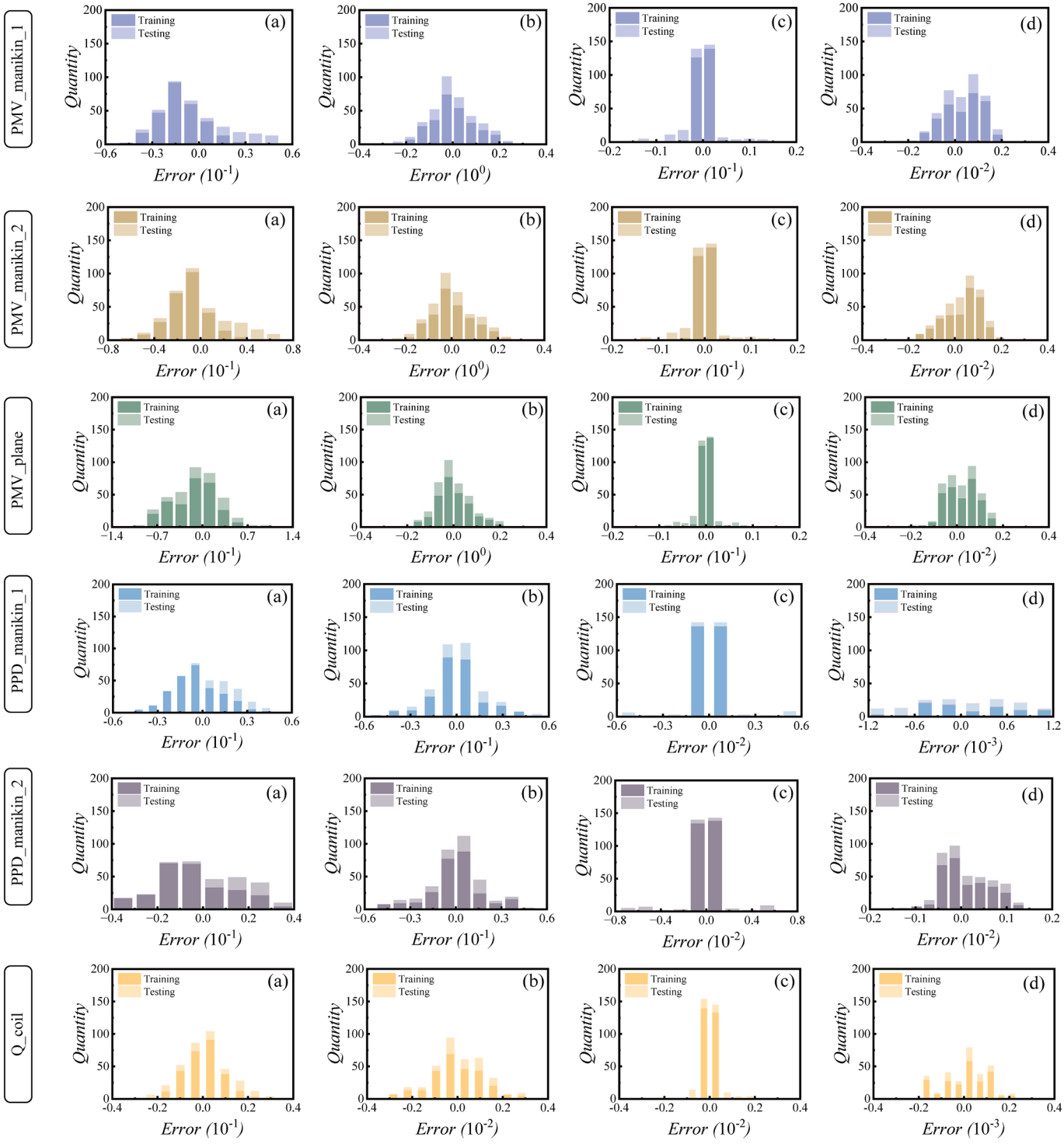

Fig. 13. Histogram-based comparison of prediction errors in thermal comfort and energy consumption by four ML algorithms, (a) BPNN, (b) CatBoost, (c) XGBboost and (d) TabPFN.

error distributions, with most errors constrained within a very narrow range, corresponding to a 1-2 orders-of-magnitude reduction compared to the other models. This highlights that TabPFN holds a clear order-of-magnitude advantage in both error magnitude and distribution compactness, demonstrating significantly higher predictive precision and stability. Such superior accuracy provides a more reliable foundation for the subsequent multi-objective optimisation purpose of indoor environmental control strategies, such as using GA or PSO algorithms.

Fig. 14 further calculated the MAE and RMSE of different models across multiple objectives. It was found that, for different prediction targets, all models performed well when predicting PMV and DR values, with MAE and RMSE remaining below 0.1275 and 0.5035, respectively. However, for other targets, including PPD, Q_coil, and the age of air, the prediction errors were significantly higher. Among the models, BPNN produced the largest errors for predicting the age of air plane, with MAE and RMSE reaching 415.7285 and 538.0678, respectively. In contrast, TabPFN demonstrated a much stronger advantage, achieving MAE and RMSE values of 4.76 and 6.81. For predicting the age of air plane, Q_{coil}, $PPD_{manikin\_1}$, and $PPD_{manikin\_2}$, compared to BPNN, TabPFN reduced the MAE by 98.96 %, 98.79 %, 98.05 %, and 98.42 %, respec-

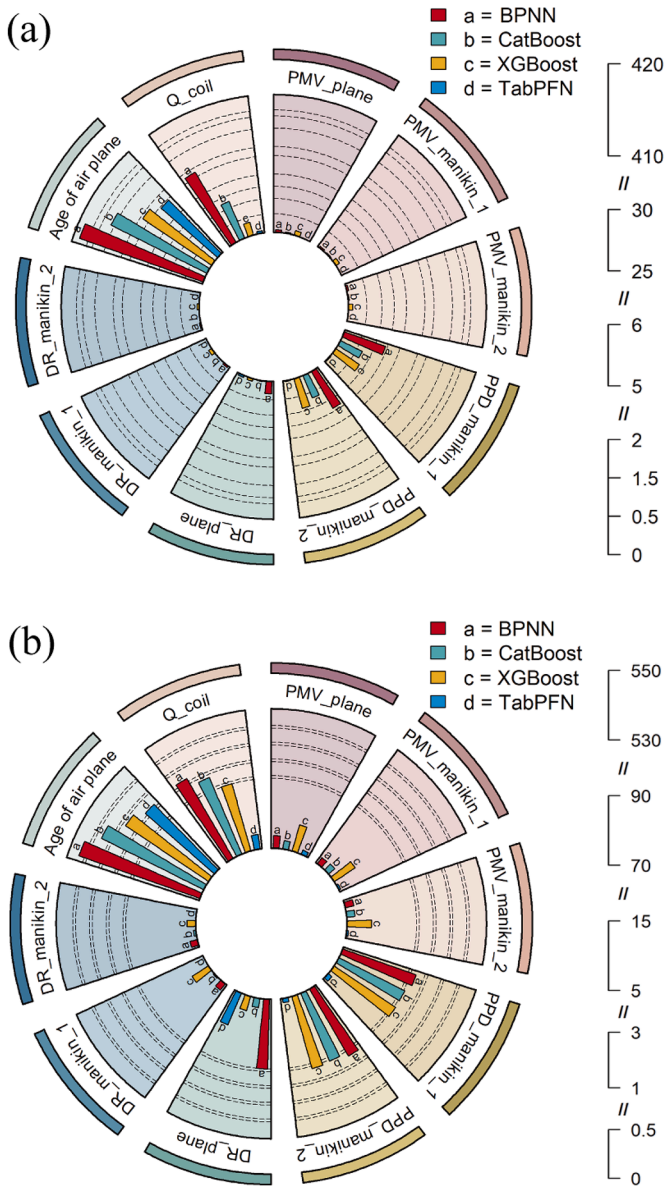

Fig. 14. MAE and RMSE evaluation of the predicted models.

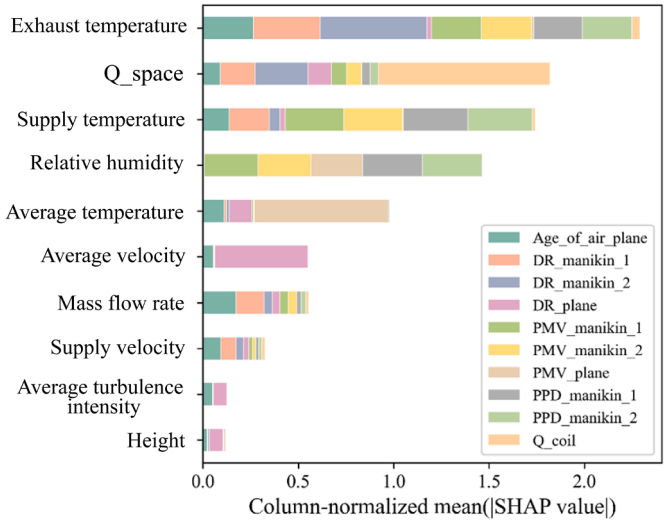

Fig. 15. Global feature importance based on column-normalised mean absolute SHAP values.

tively. Even when compared to the second-best performing model, XGBoost, TabPFN still achieved additional MAE reductions of 16.80 %, 81.59 %, 99.70 %, and 97.60 %. Overall, when considering all prediction targets, TabPFN achieved MAE reductions of 95.40 %, 62.08 %, and 80.42 % compared to BPNN, XGBoost, and CatBoost, respectively. Similarly, the RMSE was reduced by 85.50 %, 49.15 %, and 65.24 %.
This indicates that TabPFN achieves order-of-magnitude improvements in prediction accuracy, demonstrating its clear superiority on this small dataset. Such performance stems from its unique algorithmic design: unlike traditional models that rely heavily on manual hyperparameter tuning and large datasets, TabPFN employs a pre-trained transformer-based architecture specifically optimised for tabular data. This enables it to efficiently capture complex nonlinear relationships and feature interactions while requiring significantly fewer training samples. Its strong generalisation ability and adaptability to varying data distributions give TabPFN a substantial edge over conventional ML models.

In a nutshell, Table 2 outlines the ranking performance of all tested models on multi-output prediction tasks. It is evident that the TabPFN model demonstrates superior performance by striking an optimal balance between predictive accuracy and computational efficiency, achieving inference in only 6.66 s, which is approximately 85.8 % and 85.9 % faster than BPNN and CatBoost, respectively, and 67.5 % faster than XGBoost.

To improve interpretability, SHAP analysis was performed to visualise and quantify the influence of individual input factors. Fig. 15 shows the column-normalised mean global feature importance values across all prediction targets. Several consistent patterns can be observed. For instance, the supply and exhaust temperatures appear as the most influential variables across nearly all targets, which highlights the predominant role of buoyancy-driven thermal stratification in displacement ventilation. These trends are consistent with the numerical results presented in Figs. 9 and 10, which similarly show that increasing temperature can significantly influence the age of air and thermal comfort in a nonlinear manner. In addition, for the age of air, mass flow rate also contributes the most, which is consistent with its physical definition and aligns with the CFD observations, i.e., incoming flow directly influences ventilation efficiency. The PMV output is primarily affected by supply temperature and RH, reflecting the combined effects of sensible and latent heat exchange on thermal sensation. Q_space also shows strong influence on many outputs, particularly thermal comfort and energy-related predictions. In contrast, geometric and turbulence-related parameters, e.g., height, turbulence intensity, have relatively minor effects. Based on these interpretability results, it can be seen that the TabPFN model has learned physically meaningful relationships; through SHAP analysis, an overview of how input variables contribute to the multi-target prediction task can be further obtained.

In addition to the global interpretation, local SHAP explanations were applied to several representative samples to examine instance-level behavior. These plots reveal the directional influence of individual features, as shown in Fig. 16. The clustering of high (red) and low (white) feature values on opposite sides of the SHAP axis highlights the asymmetric influence of each feature, indicating that the learned mapping is nonlinear. For the age of air, it can be found that high exhaust temperatures consistently result in positive SHAP values, while increasing mass flow rate negatively impacts the age of air. For PMV, the local SHAP patterns clearly capture the expected influence of supply temperature and RH, with higher values driving positive SHAP contributions, i.e., warmer predicted sensation. A similar ranking of dominant features is observed for PPD, which is consistent with its formulation as a direct function of PMV. Overall, SHAP analysis improves model interpretability by quantifying and ranking feature contributions, capturing both the relative importance and the nonlinear, directional effects of inputs. It is

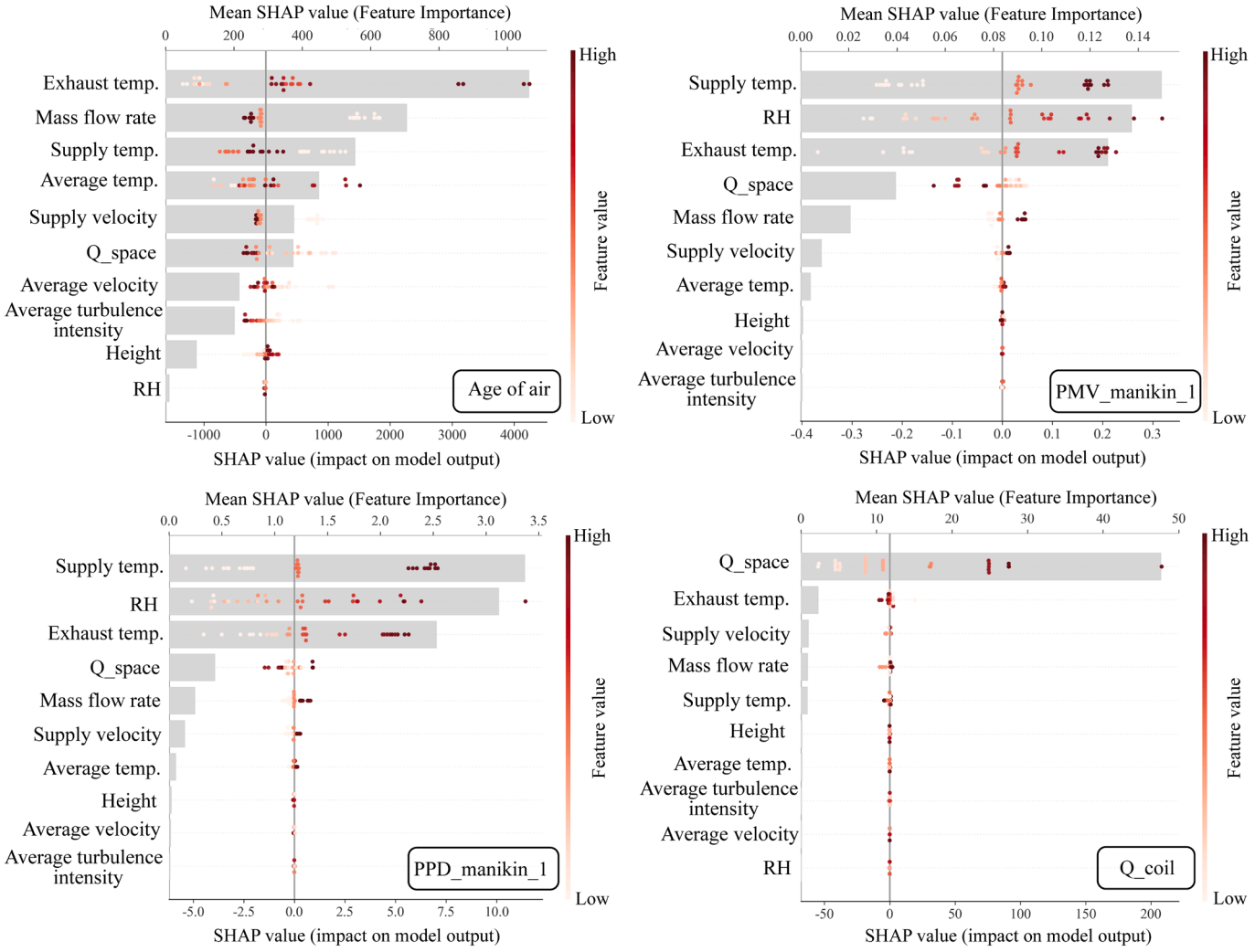

Fig. 16. Local SHAP explanations for representative prediction targets.

Table 2
Model ranking results and inference time.

Rank	Q_coil	PMV_plane	PMV_manikin_1	PMV_manikin_2	PPD_manikin_1	PPD_manikin_2	DR_plane	DR_manikin_1	DR_manikin_2	Age of air plane	Time (s)
BPNN	4	3	2	3	4	4	4	3	3	4	46.87
CatBoost	3	2	3	2	2	2	1	2	2	3	47.11
XGBoost	2	4	4	3	3	3	2	4	4	2	20.52
TabPFN	1	1	1	1	1	1	3	1	1	1	6.66

expected to provide supplemental insights for optimizing environmental control strategies.

4. Limitation

Overall, this work reveals the potential of an explainable in-context learning framework, i.e., the TabPFN-SHAP framework, as a lightweight, data-efficient surrogate model for multi-target indoor environmental performance prediction. However, this study was subject to several limitations. First, to evaluate the proposed framework's robustness, a dataset generated from validated CFD simulations under parametrised conditions was adopted, which cannot fully represent the full variability and stochasticity of real buildings. In the real-world scenario, more factors should be carefully considered, such as occupant behaviour, ventilation system dynamics, etc. Second, the relatively small dataset may also limit the generalisability of the machine-learning models. Although such a dataset is physically coherent and widely adopted in similar studies [58,59], it may still potentially constrain the model's extrapolation capability. In the future, to improve model generalisability, expanding the dataset through additional simulations and real field measurements in various indoor spaces, e.g., naturally ventilated buildings, is desirable.

5. Conclusion

In this study, an interpretable predictive framework was developed for indoor environmental management by integrating validated CFD simulations with state-of-the-art in-context learning ML models, i.e., TabPFN. A CFD dataset derived from an experimentally validated model was first established to systematically generate data for analyzing the coupled effects of ventilation parameters on IAQ, energy use and thermal sensation. An interpretable in-context learning framework integrating TabPFN and SHAP analysis was developed and trained on this dataset, aiming to predict various evaluation criteria metrics regarding air quality, comfort and energy use. TabPFN, as one of the latest models for tabular datasets, was compared with several commonly adopted benchmark models, i.e., BPNN, XGBoost, and CatBoost. The key outcomes of this study can be summarised as follows:

- The validated CFD dataset was shown to provide reliable representations of airflow and temperature distribution, with the outcomes of each indicator closely related. The dataset size remained relatively limited due to the parametric setup, which aimed to reflect the real-world challenge that multi-dimensional experimental or monitoring datasets are often scarce.
- TabPFN consistently outperformed benchmark models, achieving R^2 values close to 0.999 across multiple targets. Compared with BPNN, XGBoost, and CatBoost, TabPFN reduced MAE by up to 95.40 % and RMSE by up to 85.50 %, while also delivering 67.5-85.9 % faster inference. It is worthing mentioning that for error bins, TabFPN can achieve one to two orders of magnitude narrower than those of competing models. These improvements demonstrate the in-context learning based algorithm has much better generalisation ability computational efficiency. Therefore, it can be regarded as a robust surrogate modelling approach for complex, small-sample, multiphysics prediction problems.
- SHAP method revealed distinct dominant features for different objectives. For air quality and comfort, mass flow rate together with supply and exhaust air temperatures had the strongest influence. For thermal comfort, supply air temperature and relative humidity were the most critical factors. For energy use, exhaust air temperature emerged as the dominant driver of cooling coil load. Their nonlinear and directional effects on key indicators such as age of air, draft risk, thermal sensation, and cooling demand were quantitatively visualised, which provide interpretable physical insights into model predictions and system behavior.

CRediT authorship contribution statement

Xueren Li: Writing - original draft, Validation, Methodology, Investigation, Data curation, Conceptualization; **Weijie Sun:** Methodology, Formal analysis, Data curation, Conceptualization; **Liwei Zhang:** Writing - review & editing, Software, Methodology, Investigation, Formal analysis, Data curation; **Bichen Shang:** Writing - review & editing, Software, Methodology, Investigation, Formal analysis, Data curation; **Ruipeng Xu:** Writing - review & editing, Investigation, Methodology, Formal analysis, Data curation, Conceptualization; **Jiyuan Tu:** Writing - review & editing, Supervision; **Yuanfu Pei:** Project administration, Funding acquisition, Writing - review & editing, Software, Methodology, Investigation, Formal analysis, Data curation; **Xiang Fang:** Writing - review & editing, Project administration, Funding acquisition.

Data availability

Data will be made available on request.

Declaration of competing interest

The authors declare that they have no known competing financial interests or personal relationships that could have appeared to influence the work reported in this paper.

Acknowledgement

This research was supported by the Gansu Province Investment Project (2507-620702-04-02-798170). The authors gratefully acknowledge the support of the industrial partners Gansu Beautiful Technology Industrial Group Co., Ltd, Gansu, China, for providing valuable site information and operation data. The authors gratefully acknowledge the support of the Research Topics for 2025 of The Jiangsu Institution of Engineers (JSIE2025KT09).

Appendix A.

Table 3
Hyperparameter setup for regression NN.

Hyperparameter search space	
Hyperparameter	**Value range**
hidden_sizes	[64], [128], [256] [128, 64], [256, 128], [512, 256], [256, 256] [128, 128, 64], [256, 128, 64], [256, 256, 128]
activation	{`relu`, `gelu`, `leakyrelu`}
dropout	{0.0, 0.1, 0.2}
batchnorm	{`False`, `True`}
batch_size	{32, 64}
optimiser	{`adam`, `adamw`, `sgd`}
lr	$\{10^{-3}, 5\times10^{-4}, 10^{-4}\}$
weight_decay	$\{0.0, 10^{-5}, 10^{-4}\}$
Best hyperparameters	
Hyperparameter	**Value**
hidden_sizes	[256, 256, 128]
activation	`gelu`
dropout	0.0
batchnorm	`False`
batch_size	64
optimiser	`adamw`
lr	10^{-3}
weight_decay	10^{-5}

Table 4
Hyperparameter setup for CatBoost.

Hyperparameter search space	
Hyperparameter	**Value range**
depth	{6, 8, 10}
learning_rate	{0.03, 0.01}
l2_leaf_reg	{1, 3, 10}
rsm	{1.0, 0.8}
bootstrap_type	{`Bayesian`, `Bernoulli`}
bagging_temperature	{0.0, 1.0, 5.0} (for Bayesian)
subsample	{1.0, 0.8, 0.6} (for Bernoulli)
Best hyperparameters	
Hyperparameter	**Value**
depth	6
learning_rate	0.03
l2_leaf_reg	10
rsm	0.8
bootstrap_type	`Bernoulli`
subsample	0.8

Table 5
Hyperparameter setup for XGBoost.

Hyperparameter search space	
Hyperparameter	**Value range**
max_depth	{3, 4, 6, 8}
learning_rate	{0.03, 0.01, 0.005}
min_child_weight	{1, 3, 5}
subsample	{0.7, 0.8, 1.0}
colsample_bytree	{0.6, 1.0}
reg_alpha	{0.0, 0.1, 1.0}
reg_lambda	{1.0, 5.0, 10.0}
gamma	{0.0, 1.0}
Best hyperparameters	
Hyperparameter	**Value**
max_depth	4
learning_rate	0.03
min_child_weight	1
subsample	0.8
colsample_bytree	1.0
reg_alpha	0.0
reg_lambda	1.0
gamma	0.0

References

[1] United Nations, Department of Economic and Social Affairs, Population Division, World Urbanization Prospects 2025: The 2024 Revision, 2025, https://population.un.org/wup/, Accessed: 2026-01.

[2] M. Ji, Y. Gongxing, M. Abed Azher, E. Samia, A.K. Mohamed, J. Amin, H. Elhosiny Ali, The effect of carbon dioxide emissions on the building energy efficiency, Fuel 326 (2022) 124842. https://doi.org/10.1016/j.fuel.2022.124842

[3] X. Li, L. Zhang, B. Shang, X. Fang, Y. Tao, Y. Ma, Y. Wang, J. Tu, Thermal energy and thermo-economic analysis of PCM-TES for space heating based on low-temperature waste heat: an experimental and numerical study, Energy 311 (2024) 133286. https://doi.org/10.1016/j.energy.2024.133286

[4] Z. Guo, I. Katsamba, D. Carne, D. Feng, K. Moss, E. Barber, Z. Fang, A. Felicelli, X. Ruan, Electronic and phononic characteristics of high-performance radiative cooling pigments h-BN: a comparative study to BaSO4, Mater. Today Phys. 54 (2025) 101721. https://doi.org/10.1016/j.mtphys.2025.101721

[5] T. Al Mindeel, E. Spentzou, M. Eftekhari, Energy thermal comfort and indoor air quality: multi-objective optimization review, Renew. Sustain. Energy Rev. 202 (2024) 114682. https://doi.org/10.1016/j.rser.2024.114682

[6] A. Felicelli, Z. Yang, L. Nguyen, A. Gao, Y. Zheng, P. Li, Thin layer lightweight and ultrawhite hexagonal boron nitride nanoporous paints for daytime radiative cooling, Cell Rep. Phys. Sci. 3 (2022) 101058. https://doi.org/10.1016/j.xcrp.2022.101058

[7] L. Lu, H. Yingdong, Z. Hui, C.H. Fung Jimmy, K.H. Lau Alexis, Enhancing IAQ thermal comfort and energy efficiency through an adaptive multi-objective particle swarm optimizer-grey wolf optimization algorithm for smart environmental control, Build. Environ. 235 (2023) 110235. https://doi.org/10.1016/j.buildenv.2023.110235

[8] L. Xueren, S. Weijie, Q. Chao, Y. Yihuan, Z. Liwei, T. Jiyuan, Evaluation of supervised machine learning regression models for CFD-based surrogate modelling in indoor airflow field reconstruction, Build. Environ. 267 (2025) 112173. https://doi.org/10.1016/j.buildenv.2024.112173

[9] A. Hassan Muhammed, A. Omar, A novel adaptive predictive control strategy of hybrid radiant-air cooling systems operating in desert climates, Appl. Therm. Eng. 214 (2022) 118908. https://doi.org/10.1016/j.applthermaleng.2022.118908

[10] C. Xi, Y. Hongxing, S. Ke, A holistic passive design approach to optimize indoor environmental quality of a typical residential building in Hong Kong, Energy 113 (2016) 267–281. https://doi.org/10.1016/j.energy.2016.07.058

[11] Q. Chao, Z. Shu-Zhen, L. Zheng-Tong, W. Chih-Yung, L. Wei-Zhen, Transmission mitigation of COVID-19: exhaled contaminants removal and energy saving in densely occupied space by impinging jet ventilation, Build. Environ. 232 (2023) 110066. https://doi.org/10.1016/j.buildenv.2023.110066

[12] C. Xu, X. Zheng, F. Tian, F. Ding, S. Shen, A numerical study of the effects of exposure conditions and human movement on cough droplets transmission and deposition, Experim. Comput. Multiphase Flow 7 (4) (2025) 582–596. https://doi.org/10.1007/s42757-024-0232-z

[13] N. Clément, K. Aytaç, C. Jan, D. Dominique, CFD simulation of the wind flow under lift-up buildings using a porous approach, Build. Environ. 263 (2024) 111867. https://doi.org/10.1016/j.buildenv.2024.111867

[14] S. Mohammadreza, T. Yoshihide, CFD evaluation of mean and turbulent wind characteristics around a high-rise building affected by its surroundings, Build. Environ. 225 (2022) 109637. https://doi.org/10.1016/j.buildenv.2022.109637

[15] X. Wentao, Y. Xiao, D. Peng, K. Yanming, Z. Ke, Study of thermal and humidity environment and prediction model in impinging jet ventilation rooms based on thermal and moisture coupling, Build. Environ. 267 (2025) 112272. https://doi.org/10.1016/j.buildenv.2024.112272

[16] M.Z. Juan, B. Luca, Integrating CFD and thermoregulation models: a novel framework for thermal comfort analysis of non-uniform indoor environments, Build. Environ. 335 (2025) 115570. https://doi.org/10.1016/j.enbuild.2025.115570

[17] F. Yinshuai, F. Yu, F. Yifan, G. Jian, Effects of table based air curtains on respiratory aerosol exposure risk mitigation at face-to-face meeting setups, J. Hazardous Mater. 477 (2024) 135373. https://doi.org/10.1016/j.jhazmat.2024.135373

[18] Q. Chao, Z. Wei-Ru, F. Hong-Qiang, L. Wei-Zhen, W.M. Lee Eric, Optimization of return vent height for stratified air distribution system with impinging jet supply satisfying threshold of PMV 0.5, J. Cleaner Produc. 359 (2022) 132033. https://doi.org/10.1016/j.jclepro.2022.132033

[19] G. Hu, Q. Weixin, D. Jiankai, L. Jing, Rapid prediction of indoor airflow field using operator neural network with small dataset, Build. Environ. 251 (2024) 111175. https://doi.org/10.1016/j.buildenv.2024.111175

[20] Y. Liu, P. Ouyang, Z. Zhang, W. Xue, W. Liu, Y. Wang, H. Zhu, K. Xu, J. Lu, Multiphase flow simulation and experimental investigation of product transport during electrolyte jet machining of titanium alloy, Exper. Comput. Multiphase Flow 7 (3) (2025) 352–367.

[21] X. Li, L. Zhang, Y. Tang, Q. Chen, W. Sun, X. Fang, Y. Tao, B. Shang, Recent advances in machine learning for building envelopes: from prediction to optimization, SSRN Electron. J. (2025). https://doi.org/10.2139/ssrn.5079321

[22] S. Ghorbany, M. Hu, S. Yao, C. Wang, Q.C. Nguyen, X. Yue, M. Alirezaei, T. Tasdizen, M. Sisk, Examining the role of passive design indicators in energy burden reduction: insights from a machine learning and deep learning approach, Build. Environ. 250 (2024) 111126. https://doi.org/10.1016/j.buildenv.2023.111126

[23] M. Drass, M.A. Kraus, H. Riedel, I. Stelzer, Soundlab AI-machine learning for sound insulation value predictions of various glass assemblies, Glass Struct. Eng. 7 (1) (2022) 101–118. https://doi.org/10.1007/s40940-022-00167-z

[24] E. Golafshani, A.A. Chiniforush, P. Zandifaez, T. Ngo, An artificial intelligence framework for predicting operational energy consumption in office buildings, Energy Build. 317 (2024) 114409. https://doi.org/10.1016/j.enbuild.2024.114409

[25] H. Hosamo, B.A.C. Guilherme, C. Nordahl Rolfsen, D. Kraniotis, Building performance optimization through sensitivity analysis, and economic insights using AI, Energy Build. 325 (2024) 114999. https://doi.org/10.1016/j.enbuild.2024.114999

[26] M. Rezaie, S. Kariminia, S.S. Band, R. Ameri, M. Farokhi, H.-T. Pai, O. Gocer, B. Rismanchi, S. Shooshtarian, Energy consumption of high-rise double skin façade buildings, a machine learning analysis, J. Build. Eng. 89 (2024) 109230. https://doi.org/10.1016/j.jobe.2024.109230

[27] D. Mazzeo, N. Matera, G. Peri, G. Scaccianoce, Forecasting green roofs' potential in improving building thermal performance and mitigating urban heat island in the mediterranean area: an artificial intelligence-based approach, Appl. Therm. Eng. 222 (2023) 119879. https://doi.org/10.1016/j.applthermaleng.2022.119879

[28] W. Zhang, W. Wu, L. Norford, N. Li, A. Malkawi, Model predictive control of short-term winter natural ventilation in a smart building using machine learning algorithms, J. Build. Eng. 73 (2023) 106602. https://doi.org/10.1016/j.jobe.2023.106602

[29] Y.-S. Tsay, C.-Y. Yeh, Y.-H. Chen, M.-C. Lu, Y.-C. Lin, A machine learning-based prediction model of LCCO2 for building envelope renovation in Taiwan, Sustainability 13 (15) (2021) 8209.

[30] D. Lee, S.-T. Lee, Artificial intelligence enabled energy-efficient heating, ventilation and air conditioning system: design, analysis and necessary hardware upgrades, Appl. Thermal Eng. 235 (2023) 121253. https://doi.org/10.1016/j.applthermaleng.2023.121253

[31] X. Yu, J. Ma, F. Jiang, Revealing the impacts of the built environment factors on pedestrian-weighted air pollutant concentration using automated and interpretable machine learning, J. Environ. Manag. 387 (2025) 125850. https://doi.org/10.1016/j.jenvman.2025.125850

[32] M.L. de la Hoz-Torres, A.J. Aguilar, D.P. Ruiz, M.D. Martínez-Aires, An investigation of indoor thermal environments and thermal comfort in naturally ventilated educational buildings, J. Build. Eng. 84 (2024) 108677. https://doi.org/10.1016/j.jobe.2024.108677

[33] X. Xiao, Q. Hu, H. Jiao, Y. Wang, A. Badiei, Simulation and machine learning investigation on thermoregulation performance of phase change walls, Sustainability 15 (14) (2023) 11365.

[34] X. Xiao, Q. Hu, H. Jiao, Y. Wang, A. Badiei, Simulation and machine learning investigation on thermoregulation performance of phase change walls, Sustainability 15 (14) (2023) 11365.

[35] A.B. Daemei, E. Shafiee, A.A. Chitgar, S. Asadi, Investigating the thermal performance of green wall: experimental analysis, deep learning model, and simulation studies in a humid climate, Build. Environ. 205 (2021) 108201. https://doi.org/10.1016/j.buildenv.2021.108201

[36] P. Geyer, M.M. Singh, X. Chen, Explainable AI for engineering design: a unified approach of systems engineering and component-based deep learning demonstrated by energy-efficient building design, Adv. Eng. Inform. 62 (2024) 102843. https://doi.org/10.1016/j.aei.2024.102843

[37] G. Di Giovanni, M. Rotilio, L. Giusti, M. Ehtsham, Exploiting building information modeling and machine learning for optimizing rooftop photovoltaic systems, Energy Build. 313 (2024) 114250. https://doi.org/10.1016/j.enbuild.2024.114250

[38] C. Gnekpe, D. Tchuente, S. Nyawa, P.K. Dey, Energy performance of building refurbishments: predictive and prescriptive AI-based machine learning approaches, J. Bus. Res. 183 (2024) 114821. https://doi.org/10.1016/j.jbusres.2024.114821

[39] D.C. Nguyen, T. Asada, I. Raifuku, Y. Ishikawa, Analysis and selection of optimal perovskite/silicon tandem configuration for building integrated photovoltaics based on their annual outdoor energy yield predicted by machine learning, Solar RRL 8 (9) (2024) 2400072. https://doi.org/10.1002/solr.202400072

[40] L. Yuan, K. Sho, S. Eom, H. Nishi, D. Hasegawa, H. Zhao, T. Aoki, J. Zhu, K. Matsuo, A. Masumura, Changes in visitor behaviour across COVID-19 pandemic: unveiling urban visitation dynamics and non-linear relationships with the built environment using mobile big data, Habitat Int. 154 (2024) 103216. https://doi.org/10.1016/j.habitatint.2024.103216

[41] T. Al Mindeel, E. Spentzou, M. Eftekhari, Energy, thermal comfort, and indoor air quality: multi-objective optimization review, Renew. Sustain. Energy Rev. 202 (2024) 114682. https://www.sciencedirect.com/science/article/pii/S1364032124004088. https://doi.org/10.1016/j.rser.2024.114682

[42] A. Li, F. Xiao, Z. Xiao, R. Yan, A. Li, Y. Lv, B. Su, Active learning concerning sampling cost for enhancing AI-enabled building energy system modeling, Adv. Appl. Energy 16 (2024) 100189. https://doi.org/10.1016/j.adapen.2024.100189

[43] H. Noah, M. Samuel, P. Lennart, K. Arjun, K. Max, H.S. Bin, S.R. Tibor, H. Frank, Accurate predictions on small data with a tabular foundation model, Nature 637 (8045) (2025) 319–326. https://doi.org/10.1038/s41586-024-08328-6

[44] X. Yuan, Q. Chen, L.R. Glicksman, Y. Hu, X. Yang, Measurements and computations of room airflow with displacement ventilation, ASHRAE Trans. 105 (1999) 340.

[45] Y. Yihuan, L. Xueren, T. Yao, F. Xiang, Y. Ping, T. Jiyuan, Numerical investigation of pilots' micro-environment in an airliner cockpit, Build. Environ. 217 (2022) 109043. https://doi.org/10.1016/j.buildenv.2022.109043

[46] L. Li, Y. He, Y. Ji, J.C.H. Fung, A.K.H. Lau, Development of a mixed chamber experimental and CFD database of indoor environments, Build. Environ. 264 (2024) 111931. https://doi.org/10.1016/j.buildenv.2024.111931

[47] X. Tian, Y. Cheng, Z. Lin, Modelling indoor environment indicators using artificial neural network in the stratified environments, Build. Environ. 208 (2022) 108581. https://doi.org/10.1016/j.buildenv.2021.108581

[48] ASHRAE, Thermal Environmental Conditions for Human Occupancy, Report, The American Society of Heating Refrigerating and Air-Conditioning Engineers, 2017.

[49] L. Xueren, C. Ziqi, T. Jiyuan, Y. Hang, T. Yin, Q. Chao, Impact of impinging jet ventilation on thermal comfort and aerosol transmission: a numerical investigation in a densely-occupied classroom with solar effect, J. Build. Eng. 94 (2024) 109872. https://doi.org/10.1016/j.jobe.2024.109872

[50] L. Xueren, C. Ziqi, T. Yin, Y. Yihuan, S. Bichen, X. Shengjin, T. Jiyuan, An integrated CFD and machine learning analysis on pilots in-flight thermal comfort and productivity, Eng. Appl. Comput. Fluid Mech. 18 (1) (2024) 2421002. https://doi.org/10.1080/19942060.2024.2421002

[51] T.B. Brown, B. Mann, N. Ryder, M. Subbiah, J. Kaplan, P. Dhariwal, A. Neelakantan, P. Shyam, G. Sastry, A. Askell, S. Agarwal, A. Herbert-Voss, G. Krueger, T. Henighan, A. Rewon Child, D. Ramesh, D.M. Ziegler, J. WU, C. Winter, C. Hesse, M. Chen, E. Siger, M. Litwin, S. Gray, B. Chess, J. Clark, C. Berner, S. McCandlish, A. Radford, I. Sutekever, D. Amodei, Language models are few-shot learners, arxiv, 33 (2020) 1877-1901.

[52] C. Tianqi, G. Carlos, Xgboost: a scalable tree boosting system, in: Proceedings of the 22nd ACM Sigkdd International Conference on Knowledge Discovery and Data Mining, pp. 785–794.

[53] W. Chengjin, P. Haize, L. Zhenhua, L. Chuan, H. Hulongyi, Multi-objective optimization of residential building energy consumption, daylighting, and thermal comfort based on BO-XGBoost-NSGA-II, Build. Environ. 254 (2024) 111386. https://doi.org/10.1016/j.buildenv.2024.111386

[54] Y. Yihuan, L. Xueren, S. Weijie, F. Xiang, H. Fajiang, T. Jiyuan, Semi-surrogate modelling of droplets evaporation process via XGBoost integrated CFD simulations, Sci. Total Environ. 895 (2023) 164968. https://doi.org/10.1016/j.scitotenv.2023.164968

[55] B. Jianxiao, W. Jiarui, Y. Qian, A novel study on power consumption of an HVAC system using catboost and adaboost algorithms combined with the metaheuristic algorithms, Energy 302 (2024) 131841. https://doi.org/10.1016/j.energy.2024.131841

[56] P. Liudmila, G. Gleb, V. Aleksandr, D.A. Veronika, G. Andrey, CatBoost: unbiased boosting with categorical features, Curran Associates Inc., Red Hook, NY, USA. 2018.

[57] S.M. Lundberg, S.-I. Lee, A unified approach to interpreting model predictions, Adv. Neural Inf. Process. Syst. 30 (2017).

[58] T. Wan, Y. Bai, T. Wang, Z. Wei, BPNN-based optimal strategy for dynamic energy optimization with providing proper thermal comfort under the different outdoor air temperatures, Appl. Eenergy 313 (2022) 118899. https://www.sciencedirect.com/science/article/pii/S0306261922003257. https://doi.org/10.1016/j.apenergy.2022.118899

[59] L. Li, Y. Fu, J.C.H. Fung, K.T. Tse, A.K.H. Lau, Development of a back-propagation neural network combined with an adaptive multi-objective particle swarm optimizer algorithm for predicting and optimizing indoor CO2 and PM2.5 concentrations, J. Build. Eng. 54 (2022) 104600. https://www.sciencedirect.com/science/article/pii/S2352710222006131. https://doi.org/10.1016/j.jobe.2022.104600